Free Radical Biology & Medicine 52 (2012) 607–615

Contents lists available at SciVerse ScienceDirect

Free Radical Biology & Medicine

journal homepage: www.elsevier.com/locate/freeradbiomed

Original Contribution

Lycopene inhibits *Helicobacter pylori*-induced ATM/ATR-dependent DNA damage response in gastric epithelial AGS cells

Sung Hee Jang [a], Joo Weon Lim [a], Tomohiro Morio [b,*], Hyeyoung Kim [a,**]

[a] Department of Food and Nutrition, Brain Korea 21 Project, College of Human Ecology, Yonsei University, Seoul 120–749, Korea
[b] Department of Pediatrics and Developmental Biology, Tokyo Medical and Dental University, Graduate School of Medical and Dental Sciences, Tokyo 113–8519, Japan

ARTICLE INFO

Article history:
Received 3 June 2011
Revised 7 November 2011
Accepted 10 November 2011
Available online 20 November 2011

Keywords:
Lycopene
Helicobacter pylori
DNA damage
Gastric epithelial AGS cells
Free radicals

ABSTRACT

Oxidative stress linked to DNA damage is involved in the pathogenesis of *Helicobacter pylori*-associated gastric diseases. The DNA damage response (DDR) coordinates cell-cycle transitions, DNA repair, and apoptosis through the activation of ataxia–telangiectasia-mutated (ATM) and ATM and Rad3-related (ATR) and their target proteins. However, neither *H. pylori*-induced DDR nor the effects of antioxidants on the DNA damage have been established. This study aimed to investigate the detailed process of *H. pylori*-induced DNA damage and to examine whether lycopene, a natural antioxidant, inhibits DNA damage and cellular response of gastric epithelial AGS cells infected with *H. pylori*. AGS cells were cultured with *H. pylori* in Korean isolates and treated with or without lycopene. Cell viability, DNA damage indices, levels of 8-OH-dG, and reactive oxygen species (ROS) as well as cell-cycle distributions were determined. The activation of ATM, ATR, Chk1, and Chk2; histone H2AX focus formation; activation and induction of p53; and levels of Bax and Bcl-2 and poly(ADP-ribose) polymerase-1 (PARP-1) were assessed. The results showed that *H. pylori* induced apoptosis in AGS cells with increased Bax and decreased Bcl-2 expression as well as PARP-1 cleavage. Culture with *H. pylori* led to increases in intracellular ROS, 8-OH-dG, double-strand DNA breaks (DSBs), and DNA fragmentation. *H. pylori* induced activation of the ATM/Chk2 and ATR/Chk1 pathways, phosphorylation of H2AX and p53, and a delay in the progression of the cells entering the S phase. Lycopene inhibited *H. pylori*-induced increases in ROS, apoptosis, alterations in cell-cycle distribution, DSBs, and ATM- and ATR-mediated DDR in AGS cells. In conclusion, lycopene may be beneficial for treatment of *H. pylori*-induced gastric diseases associated with oxidative DNA damage.

Helicobacter pylori is an important risk factor for chronic gastritis, peptic ulcer, and gastric carcinoma [1]. One of the potential toxic factors involving *H. pylori*-induced gastric injury is reactive oxygen species (ROS). ROS are released from activated neutrophils and regulate signal transduction cascades, acting as key regulatory switches in many cellular processes. Because *H. pylori* exhibits chemotactic activity for neutrophils [2], the initial pathological abnormality described in *H. pylori*-induced gastritis is the neutrophil infiltration of the gastric epithelium, a hallmark of active infection. Our previous studies have shown that *H. pylori* stimulated the production of ROS in gastric epithelial cells in the absence of inflammatory cells. This increase in ROS was determined by elevated levels of lipid peroxides, an index of oxidative membrane damage [3,4]. As a source of the infected cells, our recent study showed that *H. pylori* activates NADPH oxidase by inducing translocation of heat shock protein 90β from the cytosol to the membrane, leading to the activation of Rac1, a component of the NADPH oxidase complex [5], and increases the production of ROS in gastric epithelial cells [6]. *H. pylori* directly increased transcription levels of inflammatory cytokines by activating oxidant-sensitive transcription factors NF-κB and AP-1 [7] and induced apoptosis in gastric epithelial cells [8]. Antioxidants such as mannitol, dimethylthiourea, glutathione, and β-carotene effectively suppressed the induction of IL-8 and cyclooxygenase-2 by suppressing NF-κB and AP-1 in *H. pylori*-infected gastric epithelial cells [3,9,10]. Lycopene showed antioxidant activity and inhibited IL-6 expression by suppressing NF-κB activation in pancreatic acinar cells [11]. Inhibition of ROS production by lycopene prevented a decrease in DNA repair Ku proteins and apoptosis in pancreatic acinar cells [12]. We showed that *H. pylori*-induced activation of NF-κB mediated downregulation of Bcl-2 and induced apoptosis [13], whereas the antioxidant enzyme catalase inhibited NF-κB activation and apoptotic cell death in *H. pylori*-infected gastric epithelial cells [8]. Because ROS mediate NF-κB activation, lycopene may prevent oxidant-mediated apoptosis by inhibiting NF-κB activation and downregulation of Bcl-2 in *H. pylori*-infected gastric epithelial cells.

DNA damage caused by oxidative stress may be one important factor in the pathogenesis of *H. pylori*-associated gastric diseases [14]. Two of the major regulators of the DNA damage response (DDR) are

* Corresponding author. Fax: +81 3 5803 5245.
** Corresponding author. Fax: +82 2 364 5781.
E-mail addresses: tmorio.ped@tmd.ac.jp (T. Morio), kim626@yonsei.ac.kr (H. Kim).

0891-5849/$ – see front matter © 2011 Elsevier Inc. All rights reserved.
doi:10.1016/j.freeradbiomed.2011.11.010

phosphoinositide 3-kinase-related protein kinases, ataxia–telangiectasia mutated (ATM) and ataxia–telangiectasia and Rad3-related (ATR) [15]. ATM and ATR signals control cell-cycle transitions, DNA replication, DNA repair, and apoptosis and share many biochemical and functional similarities. The major functions of ATM and ATR in cell-cycle control are redundant; however, ATM and ATR respond to different types of DNA damage. ATM responds primarily to double-strand DNA breaks (DSBs), whereas ATR reacts to the structures that contain single-stranded DNA (ssDNA). This ssDNA is generated through many different types of DNA damage such as stalled replication forks and DSBs [16–18].

Formation of DSB ends leads not only to the recruitment of the meiotic recombination protein-11 (Mre11)–Rad50–Nijmegen breakage syndrome protein-1 (Nbs1) (MRN) complex but also to conversion of dimeric ATM into monomeric phosphorylated ATM. Activated ATM then phosphorylates the C-terminal tail of the histone variant H2AX to produce γ-H2AX, the initial signal for the subsequent accumulation of DDR proteins. Activated ATM also phosphorylates other downstream targets, including checkpoint kinase 2 (Chk2). ssDNA bound to replication protein A is recognized by ATR through interaction with ATR-interacting protein and leads to activation of ATR with topoisomerase-binding protein-1. The activated ATR phosphorylates a large list of substrates including checkpoint kinase 1 (Chk1) [19]. The induction of p53 in response to DNA damage is coordinated by ATM and ATR. Both kinases phosphorylate p53 at Ser15 and other sites; stabilization of p53 is also influenced by Chk2 and Chk1, which are phosphorylated by ATM and ATR, respectively [20]. These DDRs can be elicited by ROS and culminate in cell-cycle arrest, DNA repair, and, when unrepaired, apoptosis.

H. pylori-induced DNA damage leads to the activation of p53 and apoptosis in infected cells and tissues [21,22]. *H. pylori* not only inhibits cell-cycle progression at G1–S but also causes apoptosis by inducing the expression of cyclin D1 and p53 in gastric epithelial AGS cells [23,24]. *H. pylori* releases a factor that inhibits G1-to-S progression by affecting cyclin E/cyclin-dependent kinase 2 (Cdk2) kinase activity [25]. A recent study showed that *H. pylori* γ-glutamyl transpeptidase induces apoptosis and cell-cycle arrest at the G1–S phase transition and that this induction is also associated with down-regulation of cyclin E, cyclin A, Cdk4, and Cdk6 and with upregulation of the Cdk inhibitors p27 and p21 in gastric epithelial AGS cells [26]. There have been reports on the direct effects of *H. pylori* on the inflammatory response, ROS production, cell-cycle progression, and apoptosis. However, a detailed analysis of the DDR elicited by *H. pylori* and the measures required to inhibit resulting DNA damage has not yet been explored.

Lycopene, a natural pigment synthesized by plants and microorganisms, has a high number of conjugated dienes, making it one of the most potent singlet oxygen quenchers among natural carotenoids [27]. Epidemiological studies have demonstrated that lycopene is associated with decreased risk of chronic diseases including cardiovascular diseases and cancers [28,29]. Lycopene has been shown to decrease oxidative DNA damage in lung fibroblasts [30], endothelial cells [31], and hepatocytes [32] caused by the redox cycling of catechol estrogens, H_2O_2, or γ-radiation. Lycopene also has antiproliferation and prodifferentiation activities in various types of cancer cells [33]. Therefore, lycopene has gained attention as a promising chemopreventive agent because of its antioxidant activity.

This study aimed to investigate *H. pylori*-induced DDR and the effect of lycopene on *H. pylori*-induced DNA damage in gastric epithelial AGS cells. We examined DNA damage indices (DNA fragmentation, DNA tail assessment, levels of 8-hydroxy-2′-deoxyguanosine (8-OH-dG)), levels of ROS, and alterations in the cell-cycle distribution. We also investigated the downstream events of *H. pylori*-induced activation of ATM and ATR, the expression of apoptosis-related proteins such as Bax and Bcl-2, and the cleavage of poly(ADP-ribose) polymerase-1 (PARP-1). We not only assessed the effect of lycopene on the amelioration of the reaction, but we also demonstrated that *H. pylori*-induced DDRs are caused by ROS.

Materials and methods

Bacterial strain

H. pylori in Korean isolates (HP99), the cagA$^+$, vacA s1bm2, iceA1 *H. pylori* strain [7], was inoculated onto chocolate agar plates (Becton–Dickinson Microbiology Systems, Cockeysville, MD, USA) at 37 °C under microaerophilic conditions using an anaerobic chamber (Becton–Dickinson Microbiology Systems).

Cell culture and H. pylori infection

Human gastric epithelial AGS cells (gastric adenocarcinoma, ATCC CRL 1739) were cultured in RPMI 1640 medium supplemented with 10% fetal bovine serum and penicillin/streptomycin. The cells were seeded and cultured overnight to reach 80% confluency. Before *H. pylori* infection, each well was washed once with 2 ml of fresh cell culture medium containing no antibiotics. Whole *H. pylori* was harvested from chocolate agar plates, suspended in antibiotic-free RPMI 1640 medium supplemented with 10% fetal bovine serum, and used to treat AGS cells. AGS cells were cultured in the presence of *H. pylori* at a 50:1 multiplicity of infection (m.o.i.). To investigate the effects of lycopene, the cells were treated with lycopene (Sigma, St. Louis, MO, USA) dissolved in tetrahydrofuran (final concentrations of 2 and 5 μM) for 1 h before *H. pylori* infection. The control group received tetrahydrofuran instead of lycopene. Because lycopene at 2 and 5 μM showed potent antioxidant activities in our previous studies [11,12], these concentrations were used in the present study to determine the effects of lycopene on *H. pylori*-induced DNA damage response in AGS cells.

Cell viability and DNA fragmentation

Viable cell numbers were determined using trypan blue exclusion test (0.2% trypan blue). DNA fragmentation was assessed according to the amount of oligonucleosome-bound DNA in the cell lysate using a Cell Death Detection ELISA^{plus} kit (Roche Molecular Biochemicals GmbH, Germany).

Determination of 8-OH-dG

Oxidative DNA damage was evaluated based on the generation of 8-OH-dG using a Biotrin OxyDNA assay kit (BD Biosciences, Dublin, Ireland). The formation of 8-OH-dG adducts in each sample was analyzed using flow cytometry (Beckman, Fullerton, CA, USA).

Neutral comet assay (single-cell gel electrophoresis)

Cells were suspended in 0.5% low-melting-point agarose and transferred onto a frosted glass microscope slide precoated with layer of 0.5% agarose. The slides were incubated in lysis solution (2.5 M NaCl, 100 mM Na_2 EDTA, 10 mM Trizma base, 1% *N*-lauroylsarcosine, NaOH to pH 10.0, and 1% v/v Triton X-100) at 4 °C for 1 h and electrophoresed at 25 V for 40 min. Comet tails were stained with SYBR green and analyzed by fluorescence microscope. In total, over 70 cells were analyzed per treatment using Scion Image (using scion_comet 1.3) with the comet assay for the comet tail moment.

Measurement of intracellular ROS

For the experiment on the time course of ROS production, the cells were cultured in the presence of *H. pylori* for 0, 15, 30, and 60 min. For the effects of lycopene, the cells were treated with lycopene for 1 h

before *H. pylori* infection and cultured for 1 h. At each time period, the cells were loaded with 10 μM dichlorofluorescein diacetate (DCF-DA; Molecular Probes, Eugene, OR, USA) for 30 min, washed, and scraped off into 1 ml of PBS. The fluorescent dichlorofluorescein (DCF) was measured (excitation at 495 nm and emission at 535 nm) with a VICTOR2 multilabel counter (PerkinElmer Life and Analytical Sciences, Boston, MA, USA) or a laser scanning confocal microscope (Leica TCS-NT, Heidelberg, Germany) for the experiment with lycopene.

Cell-cycle analysis

The cells were trypsinized and washed twice with cold PBS. The pellet was treated with 1% (w/v) paraformaldehyde, followed by ice-cold 70% (v/v) ethanol for at least 12 h. After two washes with PBS, the cells were incubated with RNase (200 μg/ml final concentration), stained with propidium iodide (100 μg/ml final concentration) for 30 min, and analyzed using flow cytometry on a FACSCalibur system equipped with argon ion laser (Becton–Dickinson Immunocytometry System, San Jose, CA, USA). Percentages of the cells in each phase were calculated using the Cell Modfit software program (Becton–Dickinson).

Western blot analysis

Samples containing equal amounts of protein were separated by 12% SDS–PAGE and transferred onto nitrocellulose membranes. After being blocked in 3% nonfat dry milk for 2 h, the membrane was incubated with polyclonal antibodies for phosphospecific forms of ATM, ATR, Chk1 (phospho-S345 residue), Chk2 (phospho-T68 residue), p53 (phospho-S15 residue), and H2AX (γ-H2AX, phospho-S139 residue) (all from Cell Signaling Technology, Beverly, MA, USA). Some of the other polyclonal antibodies used were total forms of Chk1, Chk2, H2AX, PARP-1 (full-length PARP-1 (116 kDa) and large fragment of PARP-1 (89 kDa)) (all from Cell Signaling Technology) and ATR, ATM, p53, Bax, Bcl-2, or actin (all from Santa Cruz Biotechnology, Santa Cruz, CA, USA) in TBS-T (Tris-buffered saline containing 0.15% Tween 20) containing 3% nonfat dry milk at 4 °C overnight. Anti-Nbs1 and anti-Rad50 antibodies were obtained from Calbiochem (San Diego, CA, USA), and anti-Mre11 polyclonal antibody was from Novus Biologicals (Littleton, CO, USA). After being washed with TBS-T, the immunoreactive proteins were visualized using goat anti-mouse secondary antibodies conjugated to horseradish peroxidase, followed by enhanced chemiluminescence (Santa Cruz Biotechnology). Actin served as a loading control. Proteins (molecular mass) used in the study were Chk1 (56 kDa), Chk2 (66 kDa), ATR (250 kDa), ATM (370 kDa), p53 (53 kDa), Bax (23 kDa), Bcl-2 (26 kDa), PARP-1 (116 kDa), cleaved PARP-1 (89 kDa), H2AX (15 kDa), Nbs1 (95 kDa), Mre11 (80 kDa), and Rad50 (150 kDa). For the ratio of Bax/Bcl-2 as a parameter of apoptotic cell death, the protein bands of Bax and Bcl-2 were scanned using a Bio-Rad scanner (GS-700) driven by volume analysis software and quantified with Molecular Analysis software (version 4.1).

Immunofluorescence analysis for γ-H2AX

The cells were fixed with cold ethanol for 10 min and permeabilized in 0.1% Triton X-100/PBS for 15 min. The cells were blocked in PBS containing 5% goat serum and 1% bovine serum albumin and then incubated with polyclonal rabbit anti-γ-H2AX antibody for 1 h, followed by rhodamine-labeled mouse anti-rabbit IgG antibody (final concentration, 2 μg/ml) for 1 h. The cells were washed with PBS and stained with 5 μg/ml DAPI (4′,6′-diamidino-2-phenylindole) for 10 min. After being washed with PBS, the cells were mounted onto diazabicyclooctane glycerol (50%) and viewed by a confocal laser scanning microscope (LSM 510 META, Carl Zeiss, Germany).The captured images were analyzed for relative quantification of γ-H2AX using ImageJ software. The DAPI-stained nucleus of each cell was selected and used for relative quantification of γ-H2AX. All the foci were counted manually.

Statistical analysis

The statistical differences were determined using one-way ANOVA and Newman–Keuls test. All values are expressed as means ± SE of four different experiments. A value of $p<0.05$ was considered statistically significant.

Results

H. pylori induces cell death and DNA damage in AGS cells

During the 24-h culture, cell viability was slightly decreased in *H. pylori*-infected cells compared with the cells without infection (Fig. 1A). With this decrease in cell viability, *H. pylori* elicited an increase in nucleosome-bound DNA, an index of DNA fragmentation (Fig. 1B). We then monitored DSBs through a neutral comet assay. Although the comet formation was evident at 12 h, it continued to increase for at least 24 h (Fig. 1C). The cells infected with *H. pylori* showed a significant increment of comet cells with increased tail moments in a time-dependent manner. The results show a time-dependent increment of DNA damage in *H. pylori*-infected cells. An elevated 8-OH-dG level is an indicator of oxidative stress as well as DNA damage [34]. Uninfected AGS cells harbored relatively low levels of 8-OH-dG formation. In contrast, there were significant increases in

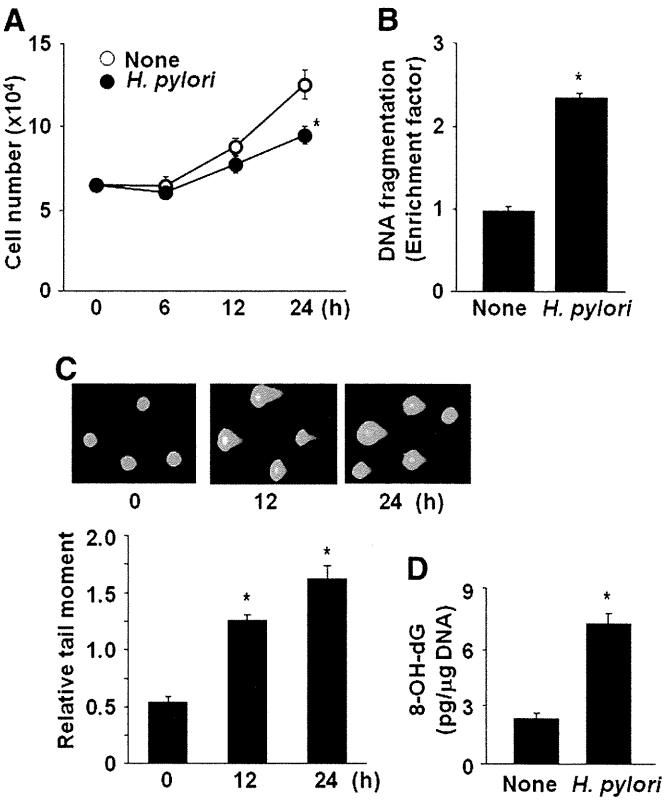

Fig. 1. *H. pylori* induces cell death and DNA damage in AGS cells. (A) Cell viability was determined using trypan blue exclusion test (0.2% trypan blue). (B) DNA fragmentation was assessed according to the amount of oligonucleosome-bound DNA in the cell lysate in 24-h culture. The relative increase in nucleosome-bound DNA, determined at 405 nm, was expressed as an enrichment factor. (C) DNA damage was examined using comet formation (top). Quantitative analysis of comet formation was assessed according to relative tail moment (bottom). (D) The levels of 8-OH-dG were analyzed fluorimetrically at 24 h culture. All values are expressed as means ± SE of four separate experiments. *$p<0.05$ for comparison to the corresponding "none" (the cells cultured in the absence of *H. pylori*) (A, B, D) or 0 h (C).

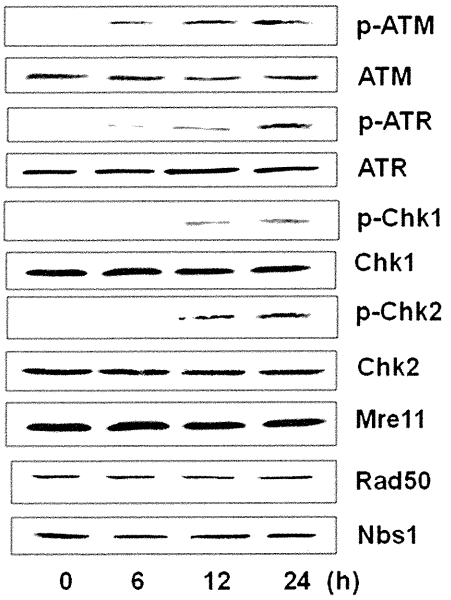

Fig. 2. *H. pylori* induces the phosphorylation of ATM, ATR, Chk1, and Chk2 in AGS cells. The levels of phosphospecific and total forms of ATM, ATR, Chk1, and Chk2 as well as total Mre11/Rad50/NBS1 were assessed using Western blot analysis, in which actin served as a loading control.

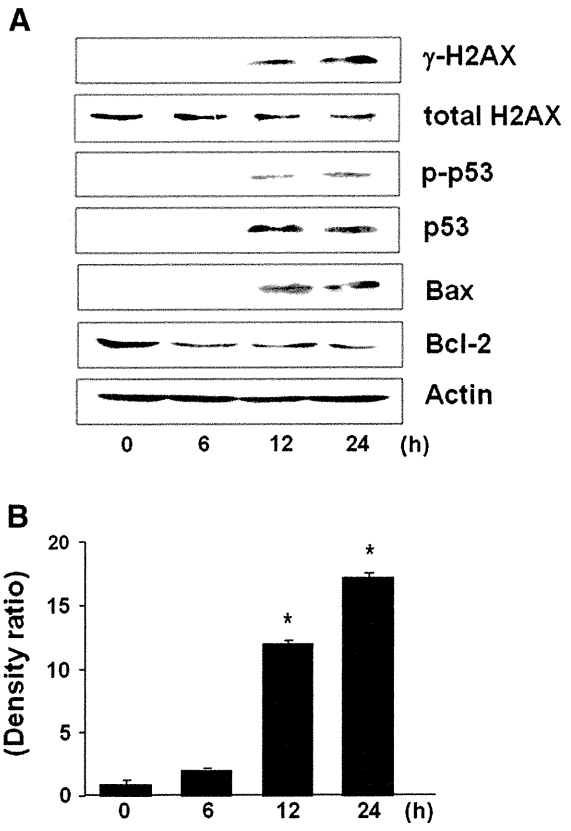

Fig. 3. *H. pylori* induces the phosphorylation of H2AX and p53 as well as alterations in the apoptotic indices of AGS cells. (A) The levels of phosphospecific and total forms of H2AX and p53 as well as apoptotic indices (Bax, Bcl-2) were determined via Western blot analysis in which actin served as a loading control. (B) The ratio of Bax/Bcl-2 was determined by the level of each protein that was scanned and expressed as density ratio. The ratio of Bax/Bcl-2 in the cells cultured in the presence of *H. pylori* at 0 h was considered as 1. All values are expressed as means ± SE of four separate experiments. *$p<0.05$ for comparison to the ratio at 0 h.

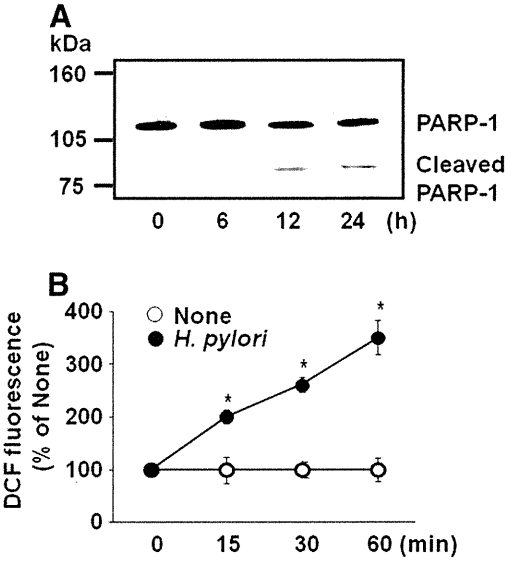

Fig. 4. *H. pylori* induces PARP-1 cleavage and an increase in ROS level of AGS cells. (A) The levels of PARP-1 (full-length PARP-1 (116 kDa) and large fragment of PARP-1 (89 kDa)) were determined via Western blot analysis. (B) ROS levels were determined by measuring the level of fluorescent DCF (excitation at 495 nm and emission at 535 nm). All values are expressed as means ± SE of four separate experiments. *$p<0.05$ for comparison to the corresponding "none" (the cells cultured in the absence of *H. pylori*).

8-OH-dG in *H. pylori*-infected AGS cells at 24 h (Fig. 1D). All of these DNA damage responses were elicited by a relatively low m.o.i. (50:1).

H. pylori induces the activation of ATM, ATR, Chk1, Chk2, H2AX, and p53

To investigate whether *H. pylori*-induced DNA damage is linked to the activation of ATM and ATR (Fig. 2), the levels of the phosphospecific and total forms of ATM and ATR as well as their target molecules such as Chk2, Chk1, and p53 were determined in *H. pylori*-infected AGS cells. The phosphorylation of ATM and ATR that was observed at 6 h increased through 24 h, whereas the total forms of ATM and ATR were not changed by *H. pylori* infection. *H. pylori* infection in AGS cells induced phosphorylation of Chk2 on T68 and Chk1 on residue S345 at 12 h, indicating the activation of ATM (Chk2) and ATR (Chk1) (Fig. 2). The total amounts of Chk2 and Chk1 as well as that of Mre11/Rad50/NBS1 were not changed by *H. pylori* infection. The phosphorylated form of H2AX (γ-H2AX) is essential to the efficient recognition and/or repair of DSBs. Phosphorylation of H2AX on S139

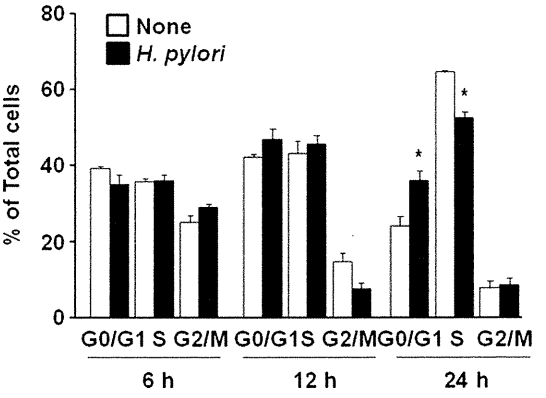

Fig. 5. *H. pylori* induces an alteration in cell-cycle distribution of AGS cells. After the cells were harvested, they were incubated with RNase and stained with propidium iodide. Flow cytometric analysis was performed to analyze the cell-cycle distribution. Percentages of the cells in each phase were calculated using the Cell Modfit software program. All values are expressed as means ± SE of four separate experiments. *$p<0.05$ for comparison to the corresponding "none" (the cells cultured in the absence of *H. pylori*).

was noted in AGS cells at 12 h, a trend that increased through 24 h (Fig. 3A). p53 is a target substrate of ATM, ATR, Chk2, and Chk1 after DDR. Phosphorylation of residue S15 of p53 was increased in *H. pylori*-infected cells (Fig. 3A) and was accompanied by the induction of p53 that is caused by stabilization of p53 protein. These results suggest that *H. pylori* induces DSBs at low m.o.i. and activates ATM and ATR DNA damage response pathways. These alterations may lead to the phosphorylation and stabilization of p53 for apoptotic cell death, alterations in cell-cycle distribution, or both.

H. pylori induces alterations in Bax and Bcl-2 as well as PARP-1 cleavage in AGS cells

p53 is known to mediate the downregulation of Bcl-2 as well as upregulation of Bax [35,36]. We next investigated the expression levels of the Bcl-2 family of apoptosis regulator proteins. As shown in Fig. 3, *H. pylori* induced an increase in Bax and a decrease in Bcl-2 (Fig. 3A) as well as an increase in the density ratio of Bax/Bcl-2 (Fig. 3B) in AGS cells. It is highly likely that the upregulation of p53 in AGS cells triggered by the DNA damage response to *H. pylori* led to the changes in the levels of Bax and Bcl-2, which then led to cellular apoptosis.

PARP-1 is involved in the DNA repair process and links DNA damage with apoptosis. Because PARP-1 is a substrate of caspase-3, PARP-1 cleavage reflects apoptotic cell death [37]. We previously showed that oxidative stress induced the activation of caspase-3 and nuclear loss of DNA repair Ku proteins in pancreatic acinar cells [38]. Therefore, ROS produced by *H. pylori* infection may activate caspase-3 and concurrently cleave PARP-1 in gastric epithelial cells. In Fig. 4A, the large fragment of PARP-1 was observed at 12 and 24 h in *H. pylori*-infected cells. The result demonstrates that PARP-1 cleavage may contribute to DNA damage and apoptosis in *H. pylori*-infected cells.

H. pylori induces increases in ROS levels in AGS cells

To determine the oxidative stress in AGS cells due to a low m.o.i. of *H. pylori*, intracellular levels of ROS were determined using DCF-DA via flow cytometry (Fig. 4B). Treatment with *H. pylori* resulted in an increase in the intracellular ROS level shown in AGS cells at 15-min culture. This increase in ROS continued for at least 60 min. These results combined with the data showing activation of the DNA damage response pathway suggest that ROS produced by *H. pylori* may mediate DNA damage and cell death in AGS cells.

H. pylori induces alterations in cell-cycle distribution of AGS cells

We then monitored whether *H. pylori* affected the cell-cycle progression in AGS cells. Flow cytometric analysis of the AGS cell distribution in the absence of *H. pylori* showed that 25, 66, and 9% of AGS cells were in the G0–G1, S, and G2–M phases at 24 h, respectively (Fig. 5). AGS cells infected with *H. pylori* showed an increase in the percentage of epithelial cells in G0–G1 from 25 to 37%, with a decrease in S phase from 66 to 52% at 24 h. After infection by *H. pylori*, AGS cells advanced quickly through the G0–G1 phase in 12 h, followed by a delay in the progression of the cells entering the S phase at 24 h. After the first 6 h, the distribution of the uninfected AGS cells showed that 39, 36, and 25% of the cells were in the G0–G1, S, and G2–M phases, respectively. These values were not significantly changed by *H. pylori* infection at 6 h culture. Lycopene itself had no effect on cell-cycle distribution of uninfected AGS cells (data not shown).

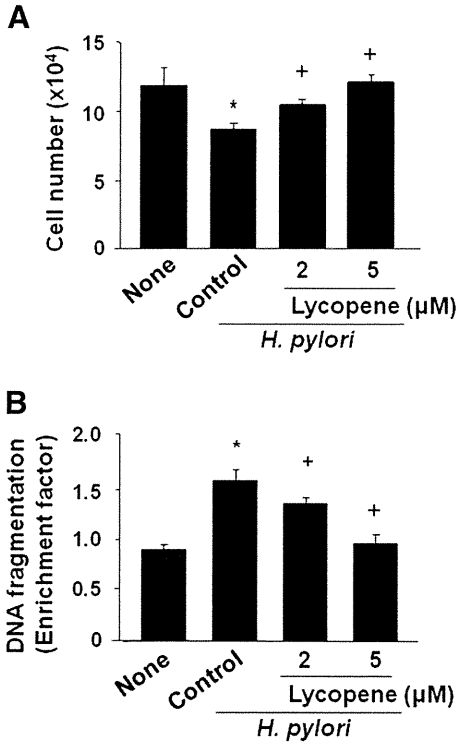

Fig. 6. Lycopene inhibits *H. pylori*-induced cell death and DNA fragmentation in AGS cells. (A) Cell viability was determined through a trypan blue exclusion test at 24 h culture. (B) DNA fragmentation was assessed according to the amount of oligonucleosome-bound DNA in the cell lysate at 24 h culture. All values are expressed as means ± SE of four separate experiments. *$p<0.05$ for comparison to "none" (the cells cultured in the absence of *H. pylori*); $^{+}p<0.05$ for comparison to control (the cells cultured in the presence of *H. pylori* without lycopene).

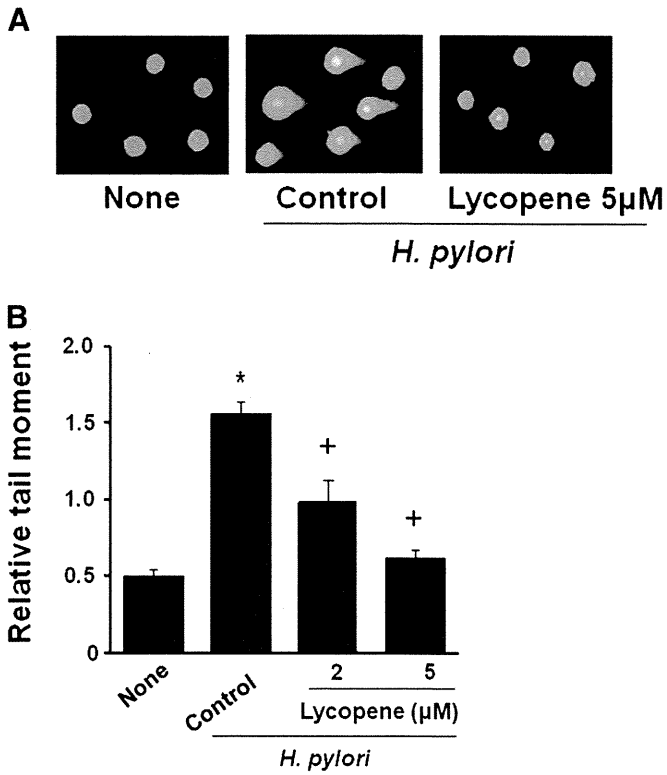

Fig. 7. Lycopene inhibits *H. pylori*-induced DNA damage in AGS cells, determined by comet assay. (A) DNA damage was examined using comet formation at 24 h culture. (B) Quantitative analysis of comet formation was assessed according to relative tail moment at 24 h culture. All values are expressed as means ± SE of four separate experiments. *$p<0.05$ for comparison to "none" (the cells cultured in the absence of *H. pylori*); $^{+}p<0.05$ for comparison to control (the cells cultured in the presence of *H. pylori* without lycopene).

Lycopene inhibits H. pylori-induced cell death, DNA damage, and γ-H2AX focus formation in AGS cells

To examine whether lycopene reverses *H. pylori*-induced DNA damage response and apoptosis, we treated *H. pylori*-infected cells with lycopene, a potent antioxidant, and monitored DNA damage responses and apoptosis. After 24 h culture, cell death and DNA fragmentation caused by *H. pylori* were inhibited by lycopene in a concentration-dependent manner (Figs. 6A and B). The addition of 5 μM lycopene almost completely inhibited *H. pylori*-induced DNA fragmentation in AGS cells. We then determined DSBs through a neutral comet assay. As shown in Fig. 7, treatment of *H. pylori* significantly increased comet formation (Fig. 7A) and tail moments (Fig. 7B) at 24 h, which was inhibited by lycopene treatment concentration dependently.

To further assess whether lycopene inhibits *H. pylori*-induced DNA damage, we examined the γ-H2AX focus formation, a commonly used in situ marker of DNA double-strand breaks, in *H. pylori*-infected cells treated with or without lycopene (Fig. 8). Immunofluorescence analysis for γ-H2AX shows that at 12 h culture, γ-H2AX focus formation was dramatically increased in *H. pylori*-infected cells. Lycopene decreased the percentage of cells exhibiting γ-H2AX foci in *H. pylori*-infected cells (Fig. 8A). The relative quantification of γ-H2AX was presented as average γ-H2AX foci per cell (Fig. 8B) and relative γ-H2AX intensity using ImageJ software (Fig. 8C). All three measures clearly demonstrate the inhibitory effect of lycopene on γ-H2AX focus formation of *H. pylori*-infected cells in a concentration-dependent manner.

Lycopene inhibits H. pylori-induced activation of ATM, ATR, Chk1, Chk2, H2AX, and p53 as well as alterations in apoptotic indices in AGS cells

The inhibitory effects of lycopene on *H. pylori*-induced phosphorylation of ATM and ATR were shown at 2 μM and were evident at 5 μM concentration of lycopene at 12 h (Fig. 9). Similarly, lycopene suppressed the phosphorylation of Chk1 on S345, Chk2 on T68, p53 on S15, and H2AX on S139, which was induced by *H. pylori* in AGS cells (Figs. 9 and 10A). The total amounts of ATM, ATR, Chk1, and Chk2 as well as the expression of the MRN complex were not changed by *H. pylori* infection with or without lycopene treatment. The induction of p53 by *H. pylori* was also suppressed by lycopene treatment.

Regarding apoptotic indices such as Bax and Bcl-2, lycopene inhibited the increase in Bax and the decrease in Bcl-2 as well as the increase in density of Bax/Bcl-2 in *H. pylori*-infected cells at 12 h (Figs. 10A and B). *H. pylori*-induced cleavage of PARP-1 was suppressed by lycopene dose dependently (Fig. 11A). Even though it is not clear whether the inhibitory effect of lycopene on the alterations in Bax and Bcl-2 are unequivocally related to the reduction of p53 induced by lycopene, the results show that *H. pylori*-induced DNA damage, the DNA damage

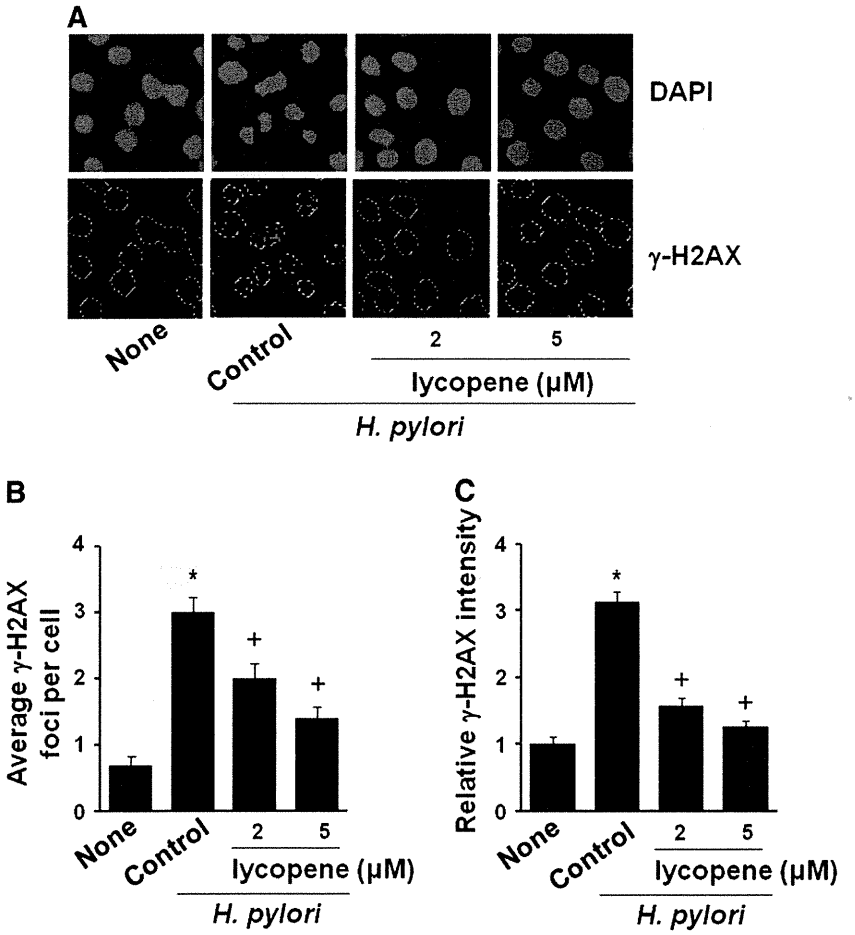

Fig. 8. Lycopene inhibits *H. pylori*-induced γ-H2AX focus formation in AGS cells. (A) At 12 h culture, the cells were stained with rabbit anti-γ-H2AX antibody and rhodamine-labeled mouse anti-rabbit IgG antibody. The cells were then stained with 5 μg/ml DAPI. The cells stained with rhodamine-labeled antibody and DAPI were examined with a laser scanning confocal microscopy. (B) Graph represents average number of γ-H2AX foci per cells. (C) Graph represents relative intensity of γ-H2AX as determined by ImageJ software. Results are expressed as means ± SE. $^{*}p<0.05$ for comparison to "none" (the cells cultured in the absence of *H. pylori*); $^{+}p<0.05$ for comparison to *H. pylori* control (the cells cultured in the presence of *H. pylori* without lycopene).

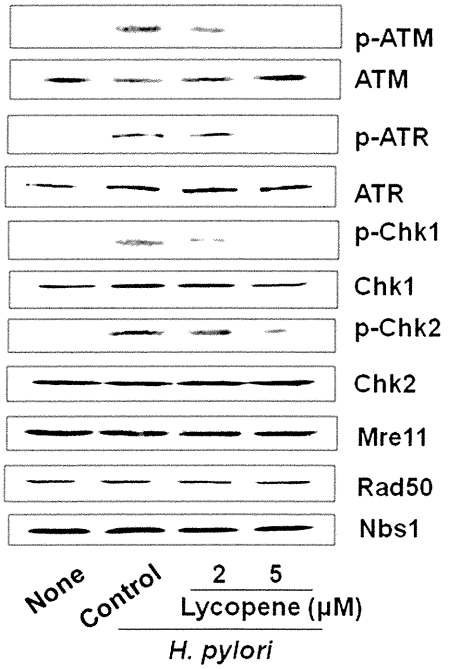

Fig. 9. Lycopene inhibits *H. pylori*-induced phosphorylation of ATM, ATR, Chk1, and Chk2 in AGS cells. At 12 h culture, the levels of phosphospecific and total forms of ATM, ATR, Chk1, and Chk2 as well as total Mre11/Rad50/Nbs1 of the cells were determined using Western blot analysis, in which actin served as a loading control.

response including the activation of ATM and ATR, and apoptosis are suppressed by lycopene treatment in AGS cells.

Lycopene inhibits the H. pylori-induced increase in ROS level and alterations in cell-cycle distribution in AGS cells

To further ensure that lycopene treatment affected ROS level in AGS cells, the intracellular levels of ROS were determined at 1 h using DCF-DA via confocal microscopy (Fig. 11B) and flow cytometry (Fig. 11C). Fig. 11 shows that the *H. pylori*-induced increase in ROS level was inhibited by lycopene in a concentration-dependent manner. Because lycopene, containing conjugated dienes, acts as a singlet oxygen quencher [27], antioxidant activity of lycopene may reduce the levels of ROS in *H. pylori*-infected AGS cells. In addition, lycopene may increase the activities and levels of antioxidant enzymes (SOD, catalase, glutathione peroxidase) in gastric epithelial cells as shown in a rat model of gastric cancer [39]. Treatment of AGS cells cultured in the presence of *H. pylori* with lycopene at a final concentration of 5 μM for 24 h decreased the proportion of cells in the G1 phase (from 37 to 26%), with a parallel increase in the proportion of cells in the S phase (from 52 to 65%) in *H. pylori*-infected AGS cells (Fig. 12), demonstrating that lycopene prevents *H. pylori*-induced delay in the progression of the cells entering the S phase at 24 h. G2–M phase was not changed in the cells, neither by *H. pylori* infection nor by lycopene treatment.

Discussion

This study demonstrates, for the first time, that *H. pylori* induces vigorous DDR that involves both ATM and ATR in a gastric epithelial cell line. Lycopene, a potent ROS-scavenging agent, rescued the *H. pylori*-infected cells from DNA damage and apoptosis.

Previously we found that *H. pylori* induced apoptosis and DNA damage in gastric epithelial cells. These inductions were suppressed by scavenging of hydrogen peroxide with catalase [8]. ROS production by *H. pylori* plays an important role in apoptosis and DNA damage processes in gastric epithelial cells [14]. Oxidative stress induces DNA damage that may well lead to apoptotic cell death, alterations in cell cycle distribution, or both. Although Chiou et al. reported that *H. pylori* inhibits G2–M to G1 progression in AGS cells [40], some studies have demonstrated that *H. pylori* and its γ-glutamyl transpeptidase inhibit cell-cycle procession at G1 and induce apoptosis [22–26]. *H. pylori*-induced p53 activation, which up-regulates the expression of p21, Bax, or both, has an important role in alterations in cell cycle distribution and apoptosis of AGS cells [22,23,41]. Recently, we found that downregulation of Bcl-2 is mediated by NF-κB activation in *H. pylori*-induced apoptosis of gastric epithelial cells [13]. In the present study, we demonstrated that *H. pylori* in Korean isolates (HP99) induced a delay in the progression of the cells entering the S phase, p53 activation, PARP-1 cleavage, upregulation of Bax, and a reciprocal decrease in Bcl-2 level in AGS cells. It is likely that p53 mediated the downregulation of Bcl-2 as well as the upregulation of Bax in *H. pylori*-infected cells, as has been shown in various cancer cells [35,36].

Some reports show that H_2O_2 and other peroxides induce ATM-dependent p53 phosphorylation in response to DNA damage, whereas others have shown that oxidative stress induces both ssDNA breaks (SSBs) and later DSBs. ATM is mainly activated by DSBs, whereas ATR

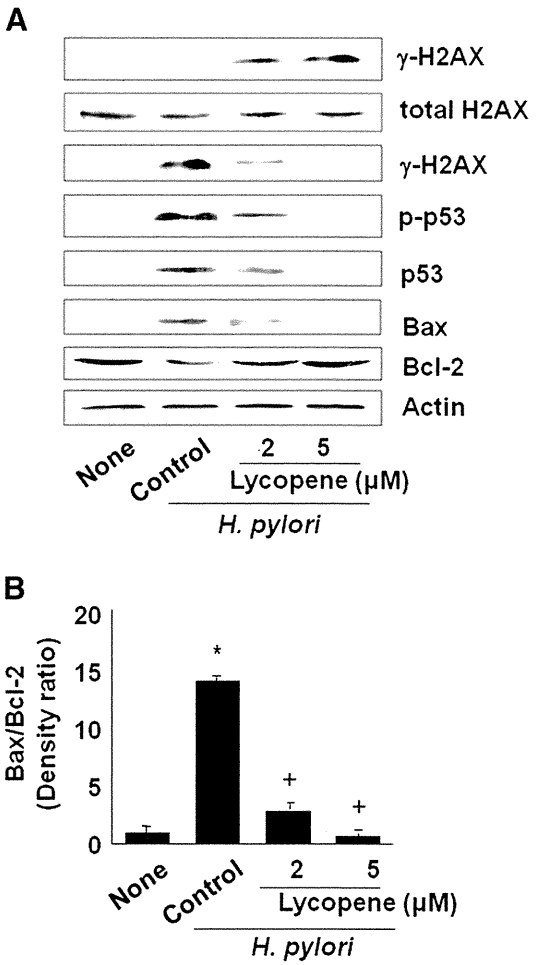

Fig. 10. Lycopene inhibits *H. pylori*-induced phosphorylation of H2AX and p53 as well as alterations in the apoptotic indices in AGS cells. (A) At 12 h culture, the levels of phosphospecific and total forms of p53 and γ-H2AX as well as apoptotic indices (Bax, Bcl-2) were assessed using Western blot analysis, in which actin served as a loading control. (B) The ratio of Bax/Bcl-2 was determined by the level of each protein, which was scanned and expressed as density ratio. The ratio of Bax/Bcl-2 in the cells cultured in the absence of *H. pylori* (none) was considered as 1. All values are expressed as means ± SE of four separate experiments. $^{*}p<0.05$ for comparison to "none" (the cells cultured in the absence of *H. pylori*); $^{+}p<0.05$ for comparison to *H. pylori* control (the cells cultured in the presence of *H. pylori* without lycopene).

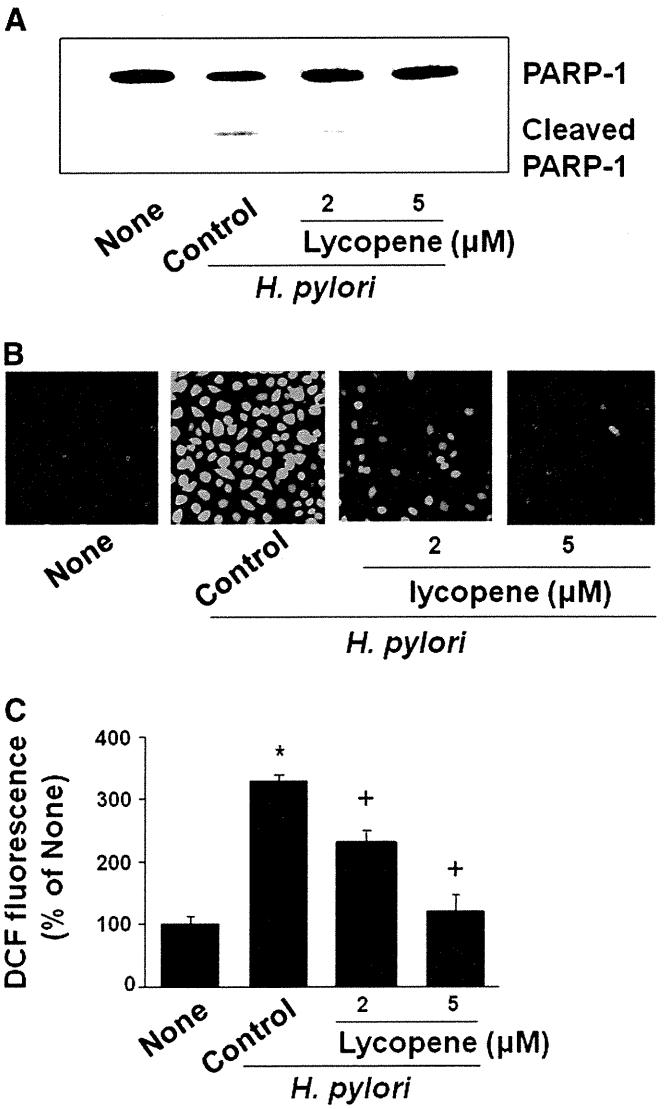

Fig. 11. Lycopene inhibits *H. pylori*-induced PARP-1 cleavage and the increase in ROS levels of AGS cells. (A) At 12 h culture, the levels PARP-1 (full-length PARP-1 (116 kDa) and large fragment of PARP-1 (89 kDa)) were determined via Western blot analysis. (B, C) At 60 min culture, ROS levels were determined using confocal microscopy (B) and by measuring the level of fluorescent dichlorofluorescein with excitation at 495 nm and emission at 535 nm (C). All values are expressed as means ± SE of four separate experiments. $^{*}p<0.05$ for comparison to the corresponding "none" (the cells cultured in the absence of *H. pylori*); $^{+}p<0.05$ for comparison to *H. pylori* control (the cells cultured in the presence of *H. pylori* without lycopene).

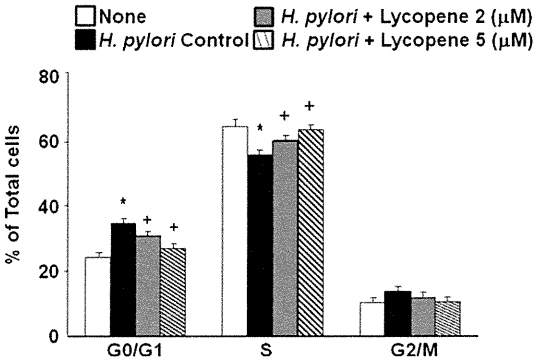

Fig. 12. Lycopene inhibits *H. pylori*-induced cell-cycle arrest in AGS cells. After the cells were harvested, they were incubated with RNase and stained with propidium iodide at 24 h culture. Flow cytometric analysis was performed to analyze the cell cycle distribution. Percentages of the cells in each phase were calculated using Cell Modfit software programs. All values are expressed as means ± SE of four separate experiments. $^{*}p<0.05$ for comparison to the corresponding "none" (the cells cultured in the absence of *H. pylori*); $^{+}p<0.05$ for comparison to *H. pylori* control (the cells cultured in the presence of *H. pylori* without lycopene).

activation is triggered by SSBs [15–18]. Although ATM and ATR affect different DNA structures, both can be activated by DSBs because DSB end resection leads to a larger single-stranded region. In that sense, ATM and ATR are considered partners in the DSB response. Our data, including a neutral comet assay, demonstrated that DSBs are generated in *H. pylori* infection and that both ATM and ATR are activated by ROS-induced DNA damage in *H. pylori*-infected gastric epithelial cells.

H2AX, one of the key components of chromatin, becomes rapidly phosphorylated on the chromatin surrounding DSBs. Phosphorylated H2AX, γ-H2AX, forms "focuses" at DSBs, which are induced by ionizing radiation, meiosis, and replication [42]. ATM is the primary kinase that phosphorylates H2AX at DSB, although ATR and DNA-dependent protein kinase have also been implicated [43]. Our present study suggests that *H. pylori*-induced γ-H2AX focus formation in gastric epithelial cells is dependent on ATM and/or ATR.

ATM activates Chk2 to stabilize and activate p53, which then affects the G1 cell-cycle checkpoint in the immortalized cells [44]. Therefore, *H. pylori* may induce alterations in cell-cycle distribution through ATM/Chk2/p53 activation in gastric epithelial cells. Because *H. pylori* induces the activation of ATR and Chk1 in AGS cells in this study, we could not exclude the involvement of ATR in *H. pylori*-induced alterations in cell-cycle distribution and apoptotic cell death. Further study should be performed to determine the relationship among ATM, ATR, other DDR proteins, and cell-cycle control proteins in *H. pylori*-infected gastric epithelial cells.

In this study, we demonstrated that lycopene at 2 and 5 μM suppressed *H. pylori*-induced DNA damage, apoptosis, and increases in ROS levels in AGS cells. Palozza et al. demonstrated that lycopene at 0.5 and 2 μM prevents the G1 cell arrest induced by oxysterol [45]. Lycopene protected against H_2O_2-induced and aflatoxin-induced DNA damage and apoptosis in human endothelial cells [31] and HepG2 cells [46]. In humans, supplementation with tomato products or purified lycopene decreased oxidative DNA damage [47]. Furthermore, consumption of tomato and tomato juice induced lymphocyte DNA resistance to oxidative stress [48]. However, little is known about the detailed effects of lycopene on oxidative stress-induced apoptosis and DNA damage.

In this study, lycopene was shown to be effective in the prevention of cellular apoptosis, a delay in the progression of the cells entering the S phase, activation of p53, and activation of ATM/ATR in *H. pylori*-infected gastric epithelial cells. Therefore, lycopene may be beneficial for the prevention and/or treatment of *H. pylori*-associated gastric diseases. This benefit may occur by inhibiting oxidative DNA damage and the consequent DNA damage response such as alterations in cell-cycle distribution and thus apoptosis through suppression of ATM/Chk2/p53 activation as well as ATR/Chk1 activation. The mechanism of lycopene may be explained at least partially by its scavenging of ROS, which prevents oxidative DNA damage and DNA strand breaks in *H. pylori*-infected gastric epithelial cells.

In summary, we have shown that *H. pylori* induces a vigorous oxidative DNA damage response involving the ATM and ATR pathways in gastric epithelial cells. The infection results in a delay in the progression of the cells entering the S phase and apoptosis. Lycopene inhibited *H. pylori*-induced DNA damage and apoptosis probably by reducing the levels of ROS and thus suppressing the DNA damage response and alterations in cell-cycle distribution in gastric epithelial cells. Lycopene may be beneficial for the prevention and the treatment of *H. pylori*-induced gastric diseases linked to oxidative DNA damage.

Acknowledgments

This study was supported by the National Research Foundation of Korea (NRF) funded by the Ministry of Education, Science, and Technology (2010–0002916, 2011–0001177) and by a grant (Joint Research Project under the Korea–Japan Basic Scientific Cooperation Program) from the NRF (F01-2009-000-10101-0) (to H.K.) and from the JSPS (to T.M.).

References

[1] Marshall, B. J. *Helicobacter pylori*. *Am. J. Gastroenterol.* **89:**S116–S128; 1994.
[2] Craig, P. M.; Territo, M. C.; Karnes, W. E.; Walsh, J. H. *Helicobacter pylori* secretes a chemotactic factor for monocytes and neutrophils. *Gut* **33:**1020–1023; 1992.
[3] Kim, H.; Seo, J. Y.; Kim, K. H. Effects of mannitol and dimethylthiourea on *Helicobacter pylori*-induced IL-8 production in gastric epithelial cells. *Pharmacology* **59:**201–211; 1999.
[4] Kim, H.; Seo, J. Y.; Kim, K. H. Inhibition of lipid peroxidation, NF-kappaB activation and IL-8 production by rebamipide in *Helicobacter pylori*-stimulated gastric epithelial cells. *Dig. Dis. Sci.* **45:**621–628; 2000.
[5] Cha, B.; Lim, J. W.; Kim, K. H.; Kim, H. HSP90beta interacts with Rac1 to activate NADPH oxidase in *Helicobacter pylori*-infected gastric epithelial cells. *Int. J. Biochem. Cell Biol.* **42:**1455–1461; 2010.
[6] Cha, B.; Lim, J. W.; Kim, K. H.; Kim, H. 15-Deoxy-$\Delta^{12,14}$-prostaglandin J_2 suppresses RANTES expression by inhibiting NADPH oxidase activation in *Helicobacter pylori*-infected gastric epithelial cells. *J. Physiol. Pharmacol.* **62:**167–174; 2011.
[7] Seo, J. H.; Lim, J. W.; Kim, H.; Kim, K. H. *Helicobacter pylori* in a Korean isolate activates mitogen-activated protein kinases, AP-1, and NF-kappaB and induces chemokine expression in gastric epithelial AGS cells. *Lab. Invest.* **84:**49–62; 2004.
[8] Lim, J. W.; Kim, H.; Kim, K. H. NF-κB, inducible nitric oxide synthase and apoptosis by *Helicobacter pylori* infection. *Free Radic. Biol. Med.* **31:**355–366; 2001.
[9] Seo, J. Y.; Kim, H.; Kim, K. H. Transcriptional regulation by thiol compounds in *Helicobacter pylori*-induced interleukin-8 production in human gastric epithelial cells. *Ann. N. Y. Acad. Sci.* **973:**541–545; 2002.
[10] Jang, S. H.; Lim, J. W.; Kim, H. Beta-carotene inhibits *Helicobacter pylori*-induced expression of inducible nitric oxide synthase and cyclooxygenase-2 in human gastric epithelial AGS cells. *J. Physiol. Pharmacol.* **60** (Suppl. 7):131–137; 2009.
[11] Kang, M.; Park, K. S.; Seo, J. Y. Lycopene inhibits IL-6 expression in cerulein-stimulated pancreatic acinar cells. *Genes Nutr.* **6:**117–123; 2011.
[12] Seo, J. Y.; Masamune, A.; Shimosegawa, T.; Kim, H. Protective effect of lycopene on oxidative stress-induced cell death of pancreatic acinar cells. *Ann. N. Y. Acad. Sci.* **1171:** 570–575; 2009.
[13] Chu, S. H.; Lim, J. W.; Kim, D. G.; Lee, E. S.; Kim, K. H.; Kim, H. Down-regulation of Bcl-2 is mediated by NF-κB activation in *Helicobacter pylori*-induced apoptosis of gastric epithelial cells. *Scand. J. Gastroenterol.* **46:**148–155; 2011.
[14] Papa, A.; Danese, S.; Sgambato, A.; Ardito, R.; Zannoni, G.; Rinelli, A.; Vecchio, F. M.; Gentiloni-Silveri, N.; Cittadini, A.; Gasbarrini, G.; Gasbarrini, A. Role of *Helicobacter pylori* $CagA^+$ infection in determining oxidative DNA damage in gastric mucosa. *Scand. J. Gastroenterol.* **37:**409–413; 2002.
[15] Yang, J.; Xu, Z. P.; Huang, Y.; Hamrick, H. E.; Duerksen-Hughes, P. J.; Yu, Y. N. ATM and ATR: sensing DNA damage. *World J. Gastroenterol.* **10:**155–160; 2004.
[16] Cann, K. L.; Hicks, G. G. Regulation of the cellular DNA double-strand break response. *Biochem. Cell Biol.* **85:**663–674; 2007.
[17] Abraham, R. T. Cell cycle checkpoint signaling through the ATM and ATR kinases. *Genes Dev.* **15:**2177–2196; 2001.
[18] Zou, L.; Elledge, S. J. Sensing DNA damage through ATRIP recognition of RPA–ssDNA complexes. *Science* **300:**1542–1548; 2003.
[19] Cimprich, K. A.; Cortez, D. ATR: an essential regulator of genome integrity. *Nat. Rev. Mol. Cell Biol.* **9:**616–627; 2008.
[20] Barzilai, A.; Yamamoto, K. DNA damage responses to oxidative stress. *DNA Repair* **3:**1109–1115; 2004.
[21] Petersson, F.; Borch, K.; Franzen, L. E. Gastric epithelial proliferation and p53 and p21 expression in a general population sample: relations to age, sex, and mucosal changes associated with *H. pylori* infection. *Dig. Dis. Sci.* **47:**1558–1566; 2002.
[22] Wei, J.; Nagy, T. A.; Vilgelm, A.; Zaika, E.; Ogden, S. R.; Romero-Gallo, J.; Piazuelo, M. B.; Correa, P.; Washington, M. K.; El-Rifai, W.; Peek, R. M.; Zaika, A. Regulation of p53 tumor suppressor by *Helicobacter pylori* in gastric epithelial cells. *Gastroenterology* **139:**1333–1343; 2010.
[23] Gao, W.; Hu, F. L.; Lü, Y. Y. *Helicobacter pylori* inhibits cell growth and induces G1/S arrest in AGS gastric epithelial cells. *Zhonghua Yi Xue Za Zhi* **83:**731–735; 2003.
[24] Shirin, H.; Weinstein, I. B.; Moss, S. F. Effect of H. pylori infection of gastric epithelial cells on cell cycle control. *Front. Biosci.* **6:**E104–E118; 2001.
[25] Sommi, P.; Svio, M.; Stivala, L. A.; Scotti, C.; Mignosi, P.; Prosperi, E.; Vannini, V.; Solcia, E. *Helicobacter pylori* releases a factor(s) inhibiting cell cycle progression of human gastric cell lines by affecting cyclin E/cdk2 kinase activity and Rb protein phosphorylation through enhanced p27(KIP1) protein expression. *Exp. Cell Res.* **281:**128–139; 2002.
[26] Kim, K. M.; Lee, S. G.; Kim, J. M.; Kim, D. S.; Song, J. Y.; Kang, H. L.; Lee, W. K.; Cho, M. J.; Rhee, K. H.; Youn, H. S.; Baik, S. C. *Helicobacter pylori* gamma-glutamyltranspeptidase induces cell cycle arrest at the G1–S phase transition. *J. Microbiol.* **48:**372–377; 2010.
[27] Di Mascio, P.; Kaiser, S.; Sies, H. Lycopene as the most efficient biological carotenoid singlet oxygen quencher. *Arch. Biochem. Biophys.* **274:**532–538; 1989.
[28] Bhuvaneswari, V.; Nagini, S. Lycopene: a review of its potential as an anticancer agent. *Curr. Med. Chem. Anticancer Agents* **5:**627–635; 2005.
[29] Rao, A. V. Lycopene, tomatoes, and the prevention of coronary heart disease. *Exp. Biol. Med. (Maywood)* **227:**908–913; 2002.
[30] Muzandu, K.; El Bohi, K.; Shaban, Z.; Ishizuka, M.; Kazusaka, A.; Fujika, S. Lycopene and beta-carotene ameliorate catechol estrogen-mediated DNA damage. *Jpn. J. Vet. Res.* **52:**173–184; 2005.
[31] Tang, X.; Yang, X.; Peng, Y.; Lin, J. Protective effects of lycopene against H_2O_2-induced oxidative injury and apoptosis in human endothelial cells. *Cardiovasc. Drugs Ther.* **23:**439–448; 2009.
[32] Srinivasan, M.; Sudheer, A. R.; Pillai, K. R.; Kumar, P. R.; Sudhakaran, P. R.; Menon, V. P. Lycopene as a natural protector against γ-radiation induced DNA damage, lipid peroxidation and antioxidant status in primary culture of isolated rat hepatocytes in vitro. *Biochim. Biophys. Acta* **1770:**659–665; 2007.
[33] Levy, J.; Bosin, E.; Feldman, B.; Giat, Y.; Miinster, A.; Danilenko, M.; Sharoni, Y. Lycopene is a more potent inhibitor of human cancer cell proliferation than either alpha-carotene or beta-carotene. *Nutr. Cancer* **24:**257r. C; 1995.
[34] Tabak, O.; Gelisgen, R.; Erman, H.; Erdenen, F.; Muderrisoglu, C.; Aral, H.; Uzun, H. Oxidative lipid, protein, and DNA damage as oxidative stress markers in vascular complications of diabetes mellitus. *Clin. Invest. Med.* **34:**E163–E171; 2011.
[35] Miyashita, T.; Harigai, M.; Hanada, M.; Reed, J. C. Identification of a p53-dependent negative response element in the bcl-2 gene. *Cancer Res.* **54:**3131–3135; 1994.
[36] Zhang, N.; Kong, X.; Yan, S.; Yuan, C.; Yang, Q. Huaier aqueous extract inhibits proliferation of breast cancer cells by inducing apoptosis. *Cancer Sci.* **101:**2375–2383; 2010.
[37] Decker, P.; Muller, S. Modulating poly (ADP-ribose) polymerase activity: potential for the prevention and therapy of pathogenic situations involving DNA damage and oxidative stress. *Curr. Pharm. Biotechnol.* **3:**275–283; 2002.
[38] Song, J. Y.; Lim, J. W.; Kim, H.; Morio, T.; Kim, K. H. Oxidative stress induces nuclear loss of DNA repair proteins Ku70 and Ku80 and apoptosis in pancreatic acinar AR42J cells. *J. Biol. Chem.* **278:**36676–36687; 2003.
[39] Luo, C.; Wu, X. G. Lycopene enhances antioxidant enzyme activities and immunity function in N-methyl-N′-nitro-N-nitrosoguanidine-induced gastric cancer rats. *Int. J. Mol. Sci.* **12:**3340–3351; 2011.
[40] Chiou, C. C.; Chan, C. C.; Kuo, Y. P.; Chan, E. C. *Helicobacter pylori* inhibits activity of cdc2 kinase and delays G2/M to G1 progression in gastric adenocarcinoma cell line. *Scand. J. Gastroenterol.* **38:**147–152; 2003.
[41] Ahmed, A.; Smoot, D.; Littleton, G.; Tackey, R.; Walters, C. S.; Kashanchi, F.; Allen, C. R.; Ashktorab, H. *Helicobacter pylori* inhibits gastric cell cycle progression. *Microbes Infect.* **2:**1159–1169; 2000.
[42] Rogakou, E. P.; Boon, C.; Redon, C.; Bonner, W. M. Megabase chromatin domains involved in DNA double-strand breaks in vivo. *J. Cell Biol.* **146:**905–916; 1999.
[43] Burma, S.; Chen, B. P.; Murphy, M.; Kurimasa, A.; Chen, D. J. ATM phosphorylates histone H2AX in response to DNA double-strand breaks. *J. Biol. Chem.* **276:** 42462–42467; 2001.
[44] Chehab, N. H.; Malikzay, A.; Appel, M.; Halazonetis, T. D. Chk2/hCds1 functions as a DNA damage checkpoint in G(1) by stabilizing p53. *Genes Dev.* **14:**278–288; 2000.
[45] Palozza, P.; Simone, R.; Catalano, A.; Boninsegna, A.; Böhm, V.; Fröhlich, K.; Mele, M. C.; Monego, G.; Ranelletti, F. O. Lycopene prevents 7-ketocholesterol-induced oxidative stress, cell cycle arrest and apoptosis in human macrophages. *J. Nutr. Biochem.* **21:**34–46; 2010.
[46] Reddy, L.; Odhav, B.; Bhoola, K. Aflatoxin B1-induced toxicity in HepG2 cells inhibited by carotenoids: morphology, apoptosis and DNA damage. *Biol. Chem.* **387:**87–93; 2006.
[47] Porrini, M.; Riso, P. Lymphocyte lycopene concentration and DNA protection from oxidative damage is increased in women after a short period of tomato consumption. *J. Nutr.* **130:**189–192; 2000.
[48] Rehman, A.; Bourne, L. C.; Halliwell, B.; Rice-Evans, C. A. Tomato consumption modulates oxidative DNA damage in humans. *Biochem. Biophys. Res. Commun.* **262:**828–831; 1999.

Biomaterials 33 (2012) 1563–1572

Contents lists available at SciVerse ScienceDirect

Biomaterials

journal homepage: www.elsevier.com/locate/biomaterials

Alleviation of rheumatoid arthritis by cell-transducible methotrexate upon transcutaneous delivery

Sang-Won Lee [a], Ji-Hye Kim [a], Min-Chan Park [a], Yong-Beom Park [a], Wook Jin Chae [b], Tomohiro Morio [c], Dong-Ho Lee [d], Sang-Hwa Yang [e], Seung-Kyou Lee [d], Soo-Kon Lee [a,**,1], Sang-Kyou Lee [d,e,*,1]

[a] Division of Rheumatology, Department of Internal Medicine, Institute for Immunology and Immunological Disease, BK21 Project for Medical Science, Yonsei University College of Medicine, 134, Shinchon-dong, Seodaemun-ku, Seoul 120-752, South Korea
[b] Department of Immunobiology, Yale University School of Medicine, New Haven, CT, USA
[c] Department of Pediatrics and Developmental Biology, Tokyo Medical and Dental University, Tokyo, Japan
[d] ForHumanTech Co., Ltd., Suwon, South Korea
[e] Department of Biotechnology, College of Life Science and Biotechnology, National Creative Research Initiatives Center For Inflammatory Response Modulation, Yonsei University, Seoul, South Korea

ARTICLE INFO

Article history:
Received 6 October 2011
Accepted 26 October 2011
Available online 17 November 2011

Keywords:
Arthritis
Drug delivery
Inflammation
Immunomodulation
Cytotoxicity

ABSTRACT

Rheumatoid arthritis (RA) is a systemic autoimmune disease that is initiated and maintained by various inflammatory/immune cells and their cytokines, leading to cartilage degradation and bone erosion. Despite its potent therapeutic efficacy on RA, the oral administration of methotrexate (MTX) provokes serious adverse systemic complications, thus necessitating the local application of MTX. Here, we show that transcutaneous MTX (TC-MTX) can efficiently penetrate joint skin *ex vivo* and *in vivo*, and that TC-MTX can significantly improve the various inflammatory symptoms associated with RA. Further, TC-MTX preserved the joint-structures in mice with collagen-induced arthritis (CIA), which was also confirmed by three-dimensional micro-computed tomography scan. TC-MTX markedly decreased the secretion of inflammatory cytokines both in the serum and in inflamed joints of CIA mice. Further, its therapeutic potential is comparable to that of etanercept, a biological agent that block tumor necrosis factor (TNF)-α. Importantly, the systemic cytotoxicity of TC-MTX was not detected. Thus, TC-MTX can be a new therapeutic modality for RA patients without systemic complications.

1. Introduction

Rheumatoid arthritis (RA) is a prototypical systemic autoimmune disease that is characterized by inflammation in multiple joints [1]. In affected joints, diverse factors initiate the emergence of RA autoantigens including type II collagen, proteoglycans, human cartilage glycoprotein, citrullinated proteins, and heat-shock proteins which then provoke a serial of immune reactions through the activation of $CD4^+$ T cells [1]. Activated $CD4^+$ T cells produce interferon (IFN)-γ and other inflammatory cytokines, which initially stimulate monocytes, macrophages and synovial fibroblasts. Subsequently, activated macrophages and synovial fibroblasts induce the overproduction of inflammatory cytokines such as tumor necrosis factor (TNF)-α, interleukin (IL)-1β, IL-6, IL-15, and IL-18 [1–3]. Activated $CD4^+$ T cells also stimulate B cells to differentiate into plasma cells producing autoantibodies including rheumatoid factor and anti-cyclic citrullinated peptide (anti-CCP) [1]. TNF-α, IL-1β and IL-6 stimulate osteoclasts, chondrocytes, neutrophils and synovial fibroblasts to produce various metalloproteinases and joint-destructive enzymes including inducible nitric oxide synthase (iNOS) and cyclooxygenase-2 (COX-2) in inflamed joints. Finally these enzymes mediate cartilage degradation and bone erosion, resulting in pain and joint destruction; in patients with inadequately treated RA, joint destruction is irreversible [1–3].

Among various disease-modifying anti-rheumatic drugs (DMARDs), the oral administration of methotrexate (MTX) is the most widely used for the treatment of RA [4–6]. MTX can slow the rate of joint destruction through its inhibitory effects on the cascade of events initiated by inflammatory cytokines and subsequent joint-destructive enzymes [7–9]. However, despite its therapeutic efficacy, the long-term administration of MTX may induce serious systemic complications, including infection, hepatitis, and bone marrow suppression [10–12]. Recently, new biological agents,

* Corresponding author. Department of Biotechnology, College of Life Science and Biotechnology, Yonsei University, 134, Shinchon-dong, Seodaemun-ku, Seoul 120-749, South Korea. Tel.: + 82 2 2123 2889, fax: + 82 2 362 7265.
** Corresponding author. Tel.: + 82 2 2228 1947, fax: + 82 2 393 6884.
1 These authors contributed equally to this work.
E-mail addresses: sookonlee@yhus.ac (S.-K. Lee), sjrlee@yonsei.ac.kr (S.-K. Lee).

0142-9612/$ – see front matter © 2011 Elsevier Ltd. All rights reserved.
doi:10.1016/j.biomaterials.2011.10.079

such as TNF-α blockade and anti-CD20 monoclonal antibody, have been developed and are being used clinically [13,14]. However, despite their potent and rapid therapeutic efficiency, these treatments may also provoke serious systemic complications, including infection, malignancies and autoimmune diseases [15,16]. Moreover, the formation of neutralizing antibodies to biological agents might decrease their therapeutic efficacy [17–19]. Therefore, it is suggested that that MTX still remains a mainstay in the treatment of RA [18].

From a clinical point of view, increasing the dose of MTX in RA patients who have several refractory small joints or continuing MTX in patients who have systemic diseases, such as pulmonary tuberculosis, interstitial lung diseases, viral hepatitis, liver cirrhosis or bone marrow dysfunction, may provoke more unwanted adverse effects. In these cases, the necessity of the local application of MTX has been raised, but to date, there has been no effective method reported to deliver MTX locally and percutaneously into joints.

In this study, we generated transcutaneous MTX (TC-MTX) to decrease the systemic toxicity of oral MTX, and to improve its therapeutic effect on affected joints. We used Franz static diffusion cells and skin from a hairless mouse, and *in vivo* in mice to confirm the effectiveness of transcutaneous delivery of MTX. TC-MTX was applied on inflamed joints of mice with collagen-induced arthritis (CIA), and both the changes in the severity of the arthritis and the levels of TNF-α, IL-1β, IL-6 and IFN-γ in inflamed joints as well as in the serum was investigated. Further, we compared the therapeutic potential of TC-MTX *in vivo* to that of the clinically used etanecept, an anti-TNF-a biological agent, for RA. Also, the toxicity of TC-MTX and its distribution in CIA mice after application was evaluated.

2. Materials and methods

2.1. Purification and generation of TC-MTX and dihydrofolate reductase (DHFR) assay

TC-MTX consists of Hph-1-PTD, ACA and MTX. First, Hph-1-PTD (YARVRRRGPRR-OH) was synthesized using solid phase techniques and commercially available fluorenyl-methoxycarbonyl (Fmoc) amino acids (Novabiochem, Darmstadt, Germany) on an Applied Biosystems 433 peptide synthesizer. ACA and MTX were coupled on the N-terminus of Hph-1-PTD sequentially. The TC-MTX conjugate was cleaved from the resin using 96% trifluoroacetic acid, 2% triisopropyl silane and 2% phenol for 12 h. Longer reaction times were necessary to completely remove the 2,2,4,6,7-pentamethyldihydrobenzofuran-5-sulfonyl group (PbfO-protecting groups) from the arginine. Subsequently, conjugates were filtered from the resin, precipitated using diethyl ether, purified using HPLC reverse-phase columns and characterized using Maldi-Tof (Bruker Daltonics, Bremen, Germany) (Fig. 1A). Because there are two carboxyl groups at α and γ positions of MTX, α and γ forms of TC-MTX were made. DHFR activity was compared to that of free MTX using a DHFR assay kit (Sigma-aldrich, Saint Louis, MO, USA) according to the manufacturer's instruction.

2.2. Franz cell experiment

A 9-mm unjacketed Franz cell with a flat flange joint and clear glass was used for the experiment [20]. Dorsal skin of hairless mice was used as a membrane. The donor chamber was filled with 10 mg of TC-MTX in 0.4 ml of 0.1 M PBS (pH 7.4) or 10 mg of MTX in 0.4 ml of 0.5 M Tris buffer (pH 10.8). The receptor chamber was filled with 4.6 ml of PBS. They were incubated at 37 °C while stirring. MTX and TC-MTX residues (MTX-ACA-tyrosine-alanine) were collected from the receptor chamber with 5 h interval until 25 h and their permeated amount were measured by HPLC.

2.3. Fluorescence microscopic analysis of penetration of TC-MTX

For the Cy5.5 labeling of TC-MTX, N-hydroxy succinimide (NHS) Cy5.5 (GE healthcare, Buckinghamshire, UK) was coupled in N-methyl pyrolidone (NMP) solution for 5 h on the side chain of lysine that was added at the N-terminal end of Hph-1-PTD. The cleavage, purification, and characterization were performed using the same processes of TC-MTX synthesis. We percutaneously applied 1% Cy5.5-labeled TC-MTX on the joint of DBA/1 mice and obtained joint tissues at 3, 6 and 24 h after application. Cy5.5 fluorescence was detected using confocal microscopy.

2.4. Induction of CIA and assessment of arthritis severity

All animals were treated in accordance with the guidelines and regulations for the use and care of animals of Yonsei University, Seoul, Korea. Arthritis was induced in DBA/1 mice at 8 weeks of age (SLC, Shizoka, Japan) and the severity of arthritis was assessed as described in our previous study [21].

2.5. Treatment protocol for CIA

Treatment began 4 weeks after the primary immunization and lasted 5 weeks. TC-MTX was mixed with sterile ointment at concentrations of 0.1%, 0.5% and 1% (mass/mass), and applied on the paws and knee joints of CIA mice in TC-MTX-treated groups in a total volume of 200 μl, twice per week. MTX was also mixed with ointment at a concentration of 1% (mass/mass) and administered to CIA mice in the percutaneous MTX-treated group with the same volume twice per week. Thirty-five mg/kg of MTX was intrapenitoneally injected into CIA mice in the intraperitoneal MTX-treated group twice per week. All mice except intraperitoneal MTX-treated mice received intraperitoneal PBS injections twice per week. Sterile ointment without MTX or TC-MTX in the same volume was applied percutaneously to controls, untreated CIA mice and intraperitoneal MTX-treated CIA mice, twice per week. To compare the *in vivo* therapeutic efficacy of TC-MTX to that of TNF-α blockade, etanercept (a recombinant TNF receptor (p75)-Fc fusion protein), (Wyeth, Madison, NJ, USA), we applied 1% TC-MTX and 1% MTX on the paws and legs of CIA mice, and we intraperitoneally injected etanercept (5.5 mg/kg) and MTX (35 mg/kg) into CIA mice at week 4, twice per week, for 5 weeks as described above.

2.6. Histopathological and immunohistochemical examination

Paws and knee joint-sections were prepared and stained with H&E and sequentially incubated with specific antibodies directed against murine TNF-α, IL-1β, IL-6, iNOS or COX-2 (SantaCruz Biotechnology, Santa Cruz, CA, USA) followed by the appropriate secondary antibodies (ISU Abxis, Seoul, Korea); expression was evaluated as described in our previous study [21].

2.7. Micro-computed tomography (CT) imaging

A total of 35 mice were used for micro-CT imaging experiments. They were evenly divided them into 5 groups (controls, untreated, and percutaneous 0.1%, 0.5% and 1% TC-MTX-treated CIA mice). The paws obtained from experimental mice were scanned, reconstructed into the three-dimensional structure with micro-CT (Skyscan 1076) (SKYSCAN, Kontick, Belgium) and evaluated as described in a previous study [21].

2.8. Measurement of serum level of TNF-α, IL-1β, IL-6 and IFN-γ

Male DBA/1 mice at 8 weeks of age (SLC, Shizoka, Japan) were evenly divided into 4 groups (controls, untreated, percutaneous 0.1% and 1% TC-MTX-treated CIA mice). The induction of arthritis, the treatment schedules, and animal sacrifice were all done according the same protocol mentioned above. The TNF-α, IL-1β, IL-6 and IFN-γ concentrations in the experimental CIA mice serum were measured by the sandwich ELISA (SantaCruz Biotechnology, Santa Cruz, CA, USA) performed according to the manufacturer's instructions.

2.9. Distribution and toxicity of percutaneously administered TC-MTX in CIA mice

We applied 5 mg/kg of TC-MTX conjugated with radioactive ^{14}C on the skin of mice and sacrificed mice at 1, 4, 24, 48 or 120 h after application. Skin from the application sites, kidney and liver of mice were harvested, and the concentration of radioactivity was determined with a radioactivity detector. Concentrations are presented as ng.eq/g of TC-MTX. Blood samples taken at the time of sacrifice from controls, and 0.1% or 1% TC-MTX-treated CIA mice were examined for white blood cell (WBC) count, hemoglobin (Hb), platelet (PLT) count, and the levels of aspartate aminotransferase (AST), alanine aminotransferase (ALT), blood nitrogen (BUN) and creatinine (Cr) to determine liver and kidney toxicity. To confirm the histopathological changes in the skin of CIA mice treated with TC-MTX, two pathologists and one dermatologist examined sections of joints; samples were blinded to prevent unconscious bias. Histological parameters included hyperkeratosis (thickening of the stratum corneum), parakeratosis, spongiosis and exocytosis and these parameters were scored as follows: 0 = normal; 1 = equivocal; 2 = mild; 3 = moderate; and 4 = severe [22].

2.10. Statistics

All statistical analyses were conducted using SPSS package for Windows, version 15 (SPSS Inc., Chicago, IL, USA). All results and measurements are expressed as the mean ± standard deviation. Statistical analysis of group differences was examined using the Mann-Whitney *U* test and a *t*-test. Correlations were calculated using Spearman's correlation coefficient. $^{*}P < 0.05$ was considered to be significant.

3. Results

3.1. Inhibition of DHFR activity by TC-MTX and its percutaneous delivery

To generate a TC-MTX that could facilitate the percutaneous delivery of MTX, we sequentially conjugated 6-amino cupric acid (ACA) and Hph-1-Protein Transduction Domain (PTD) to a carboxyl group of MTX. In TC-MTX, ACA, a small and flexible spacer, was inserted to allow MTX to interact with the binding pocket of dihydrofolate reductase (DHFR) without steric hindrance (Fig. 1A). To eliminate the concern that the chemical conjugation of MTX could influence the interaction between MTX and DHFR, the inhibitory potential of TC-MTX on DHFR activity was compared

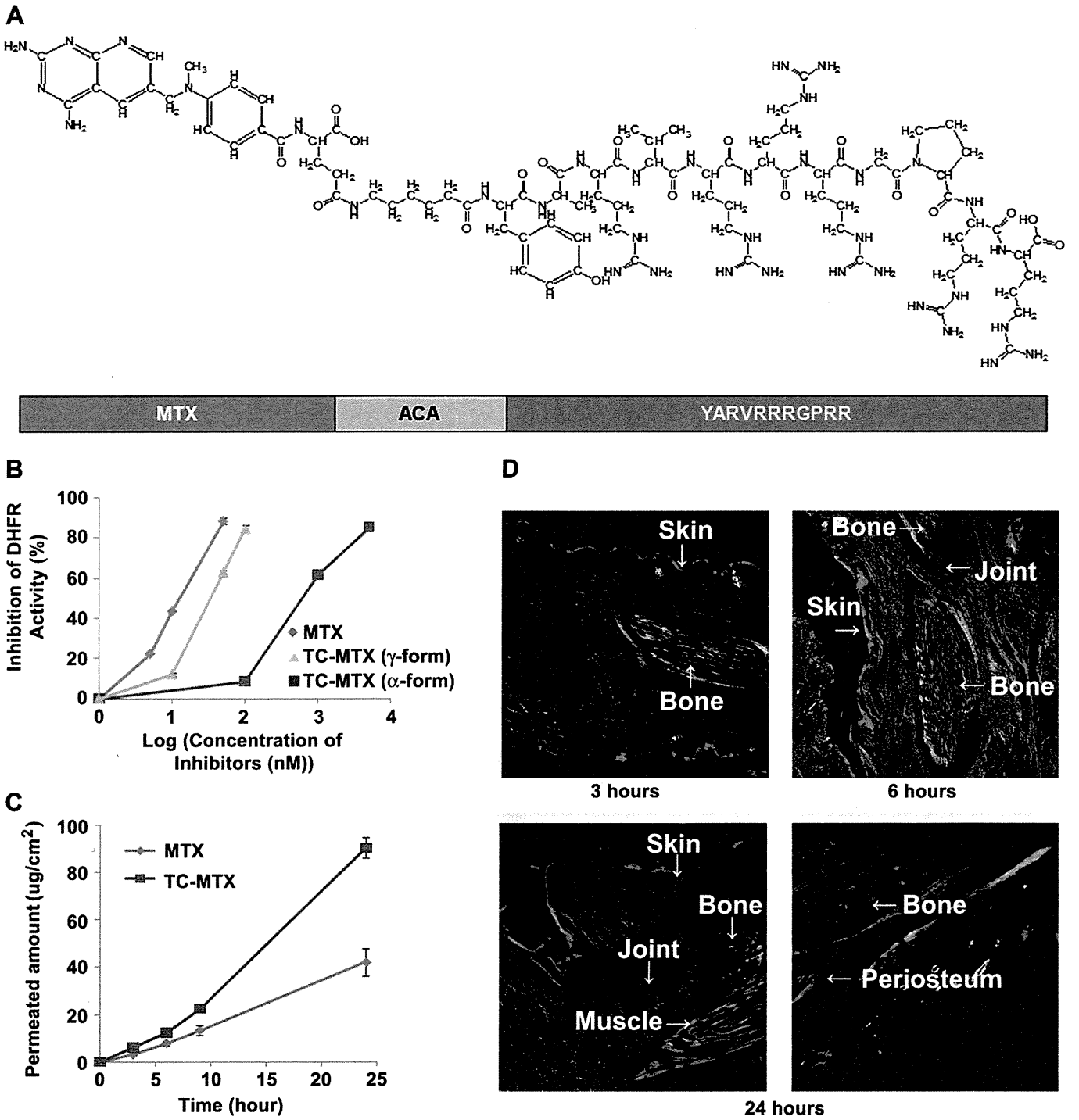

Fig. 1. Percutaneous delivery kinetics of transcutaneous MTX (TC-MTX). MTX was sequentially conjugated with ACA and Hph-1-PTD (A). The inhibitory potential of TC-MTX, α and γ forms) on DHFR activity was compared with that of free MTX using a DHFR assay kit (B). The skin-penetrating efficiency of TC-MTX was examined in a Franz cell experiment using the dorsal skin of hairless mice (C). Cy5.5-labeled TC-MTX was applied on the skin of paws and legs of mice. Cy5.5 was detected using confocal microscopy at 3, 6, and 24 h after application (original magnification×100) (D).

with that of free MTX using a DHFR assay kit. There are two carboxyl groups (α and γ positions) available for chemical conjugation in MTX. The γ form of TC-MTX inhibited DHFR activity more efficiently than the α form of TC-MTX and its inhibitory activity was comparable to that of free MTX. The half maximal inhibitory concentration (IC50) of the α and γ forms of TC-MTX and free MTX were 813 nM, 51.7 nM and 23.6 nM, respectively (Fig. 1B). Therefore, the γ form of TC-MTX was chosen for the evaluation of the therapeutic potential of TC-MTX upon percutaneous delivery. To examine the skin-penetrating efficiency of TC-MTX, we conducted experiments using the dorsal skin of hairless mice and Franz cells [20]. The donor chamber was filled with 10 mg of TC-MTX dissolved in phosphate-buffered saline (PBS, pH 7.4) or 10 mg of MTX dissolved in Tris buffer (pH 10.8). The permeated amount in the receptor chamber was measured by high performance liquid chromatography (HPLC) at 5 h interval until 25 h. The skin-penetrating efficiency of TC-MTX was significantly higher than that of MTX (Fig. 1C). To test whether TC-MTX can be delivered into joints *in vivo*, we applied TC-MTX labeled with Cy5.5 on the skin of the paws and legs of mice and examined fluorescence in joint-sections at 3, 6 or 24 h after the application. While Cy5.5 was confined to the skin and muscle layers at 3 and 6 h, strong Cy5.5 fluorescence was detected in the periosteal and periarticular tissues at 24 h, thus demonstrating the time-dependent skin-penetrating efficiency of TC-MTX (Fig. 1D). Taken together, these data demonstrate that TC-MTX efficiently and specifically penetrate into the joints through the skin *in vivo*.

3.2. The severity of arthritis by TC-MTX in vivo

To assess the therapeutic activity of TC-MTX on arthritis, we applied TC-MTX (0.1%, 0.5% or 1%) or MTX percutaneously on the paws and legs of CIA mice, or intraperitoneally injected MTX at week 4, twice a week for 5 weeks. Controls were normal mice which did not received type II collagen. Macroscopic evidence of arthritis such as erythema or swelling was clearly observed in untreated and percutaneous MTX-treated CIA mice. In contrast, percutaneous TC-MTX significantly decreased both mean arthritis score and paw thickness in a dose-dependent manner (Fig. 2A). The histopathological evaluation of the joint-sections of untreated and percutaneous MTX-treated CIA mice revealed inflammatory cell infiltration, synovial hyperplasia, and partial bone destruction. However, in CIA mice percutaneously treated with TC-MTX, the severity of the observed pathological changes was significantly reduced (Fig. 2B and C). With these results, we conclude that TC-MTX can be delivered through the skin into the joints, where it can effectively inhibit inflammatory cell infiltration and markedly alleviate arthritis in CIA mice.

3.3. The therapeutic efficiency of TC-MTX analyzed by Micro-CT

We performed three-dimensional micro-CT imaging analysis to quantitatively investigate the level of bone alterations. Severe bone destruction was observed in untreated CIA mice, but TC-MTX-treated CIA mice exhibited the dose-dependent preservation of bone integrity; the examination of bones in 1% TC-MTX-treated CIA mice found them to be comparable to naïve mice without arthritis (Fig. 3A). Four parameters were analyzed: bone volume (BV), bone volume/tissue volume (BV/TV), bone surface areas adjusted to BV (BS/BV) and trabecular thickness (Tb.Th). The BV and BV/TV measurements allowed us to compare the bone samples of different sizes, when determining the extent of bone preservation. The BS/BV parameter reflects the loss of bone surface due to erosion. Tb.Th is inversely correlated with periarticular osteopenia induced by joint inflammation [23]. TC-MTX-treated CIA mice showed significantly higher BV, BV/TV, Tb.Th and lower BS/BV values in a dose-dependent manner compared to those in untreated mice (Fig. 3B). To clarify the validity of these parameters, we evaluated the correlation coefficiencies among four parameters, and found that Tb.Th was correlated with BV/TV and BS/BV ($r^2 = 0.757$ and $r^2 = -0.698$, $p < 0.001$, respectively), and that BV/TV was also well correlated with BS/BV ($r^2 = -0.925$, $p < 0.001$) (Fig. 3C). With these results, we conclude that TC-MTX can effectively alleviate arthritis and preserve bone volume and integrity in CIA mice. To clarify the validity of these parameters, we evaluated the correlation coefficiencies among four parameters, and found that Tb.Th was correlated with BV/TV and BS/BV ($r^2 = 0.757$ and $r^2 = -0.698$, $p < 0.001$, respectively), and that BV/TV was also well correlated with BS/BV ($r^2 = -0.925$, $p < 0.001$) (Fig. 3D). These results suggest that TC-MTX can effectively preserve bone volume and integrity in CIA mice.

3.4. Reduction of inflammatory cytokines by TC-MTX

In inflamed joints, the inflammatory cytokines TNF-α, IL-1β, and IL-6, and the joint-destructive enzymes iNOS and COX-2 are the pivotal messengers in the pathophysiology of RA [1,2,8]. To examine whether TC-MTX could modulate the expression of inflammatory cytokines and enzymes in inflamed joints, we performed immunohistochemistry on the joint-sections of CIA mice. The immunohistochemical analysis of the joint-sections of untreated and percutaneous MTX-treated CIA mice showed positive staining for TNF-α, IL-1β, IL-6, iNOS, and COX-2. In contrast, TC-MTX significantly reduced their expression in a dose-dependent manner. The extent of the expression of TNF-α, IL-1β, IL-6, iNOS, and COX-2 in CIA mice percutaneously treated with 0.5% or 1% TC-MTX was equivalent to that in CIA mice intraperitoneally injected with MTX or controls (Fig. 4A and B). No positive immunohistochemical staining was detected in joint-sections, when isotype-matched irrelevant antibodies were used as controls (Supplementary material, S1). The serum concentrations of inflammatory cytokines have a tendency to be proportional to the extent of joint inflammation in CIA mice [24,25].

To investigate whether TC-MTX could decrease serum levels of inflammatory cytokines, we measured the concentrations of TNF-α, IL-1β, IL-6 and IFN-γ in the serum of CIA mice percutaneously treated with 0.1% or 1% TC-MTX. TC-MTX significantly reduced serum concentrations of these cytokines in a dose-dependent manner. In comparison with untreated CIA mice, 1% TC-MTX reduced concentrations of these inflammatory cytokines in the serum by over 70% (Fig. 4C). Taken together, TC-MTX can significantly decrease levels of inflammatory cytokines in the serum and in inflamed joints of CIA mice. Further, TC-MTX significantly reduced levels of joint-destructive enzymes within inflamed joints of CIA mice.

3.5. Comparison of therapeutic efficacy between TC-MTX and etanercept

To compare the *in vivo* therapeutic efficacy of TC-MTX to that of a TNF-α blockade, etanercept, we percutaneously applied 1% MTX or 1% TC-MTX on the paws and legs of CIA mice, and intraperitoneally injected etanercept (5.5 mg/kg) or MTX (35 mg/kg) into CIA mice, twice per week for 4 weeks for 5 weeks. We assessed arthritis score, paw thickness, and histopathological alterations in these mice. Significant joint inflammation was observed in untreated CIA mice or CIA mice percutaneously treated with MTX. Mean arthritis score and paw thickness results revealed that the therapeutic efficacy of 1% TC-MTX was almost equivalent to that of intraperitoneally injected-etanercept or -MTX (Fig. 5A). Also TC-MTX and etanercept significantly decreased histopathological alterations including inflammatory cell infiltration and bone erosion to similar

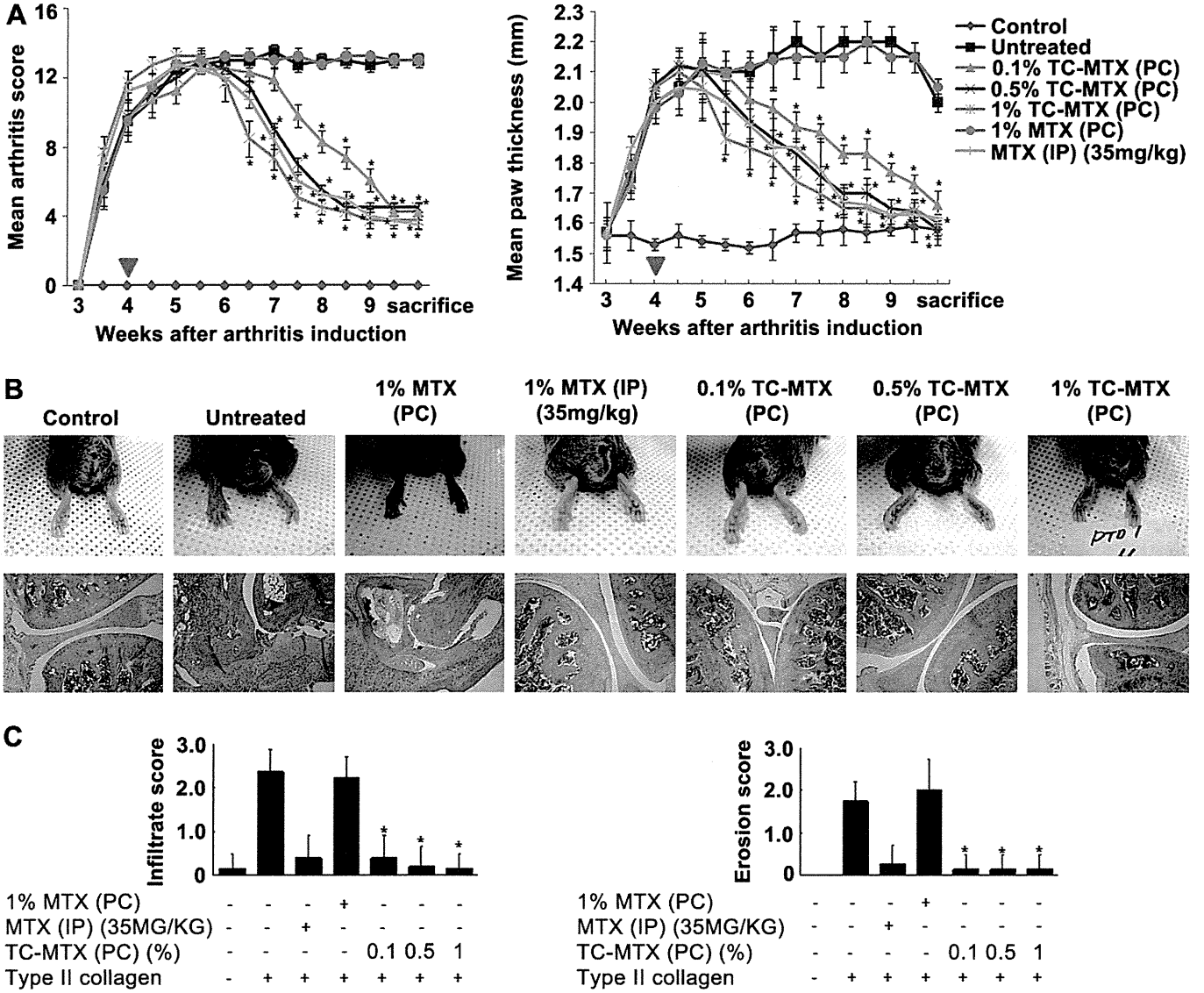

Fig. 2. Dose-dependent reduction of the severity of arthritis in CIA mice by transcutaneous MTX (TC-MTX). Percutaneous TC-MTX (0.1%, 0.5% or 1%) or MTX and intraperitoneal MTX were applied on day 28 after primary immunization (red ▼), twice per week for five weeks. Controls were normal mice which did not received type II collagen. Macroscopic evidence of arthritis such as erythema or swelling was assessed by arthritis score and paw thickness. (PC, percutaneous; IP, intraperitoneal) (A). Macroscopic and histological findings of the joint-sections were evaluated (original magnification × 100). (B : bone, C : cartilage, ST : synovial tissue) (B). The semi-quantitative analysis of histological findings of the inflamed joints including infiltrate score and erosion score (C). Values are given as mean ± SD, $n = 5$, asterisks represent significance compared to untreated mice with $^{*}p < 0.05$. (For interpretation of the references to colour in this figure legend, the reader is referred to the web version of this article.)

degrees (Fig. 5B and C). We conclude that the therapeutic efficacy of TC-MTX on arthritis in CIA mice is comparable to that of etanercept.

3.6. *In vivo distribution and cytotoxicity of TC-MTX*

To examine the distribution of percutaneously applied TC-MTX, we labeled the ACA linker with radioactive ^{14}C, and then applied 5 mg/kg of radio-labeled TC-MTX on the skin of the shaved right thighs of mice. The concentration of radioactivity in the application site (skin), kidney and liver was examined at different time points after administration. A high concentration of radioactivity was detected at the application site during the entire experimental period with peak levels at 48 h. In contrast, very low levels of radioactivity were detected in kidney and liver at 24 and 48 h, with no radioactivity being detected at 120 h (Table 1). We conclude that the majority of TC-MTX stays and exert its effects at the application site, and its contribution to the systemic circulation is minimal. To evaluate the toxicity of TC-MTX *in vivo*, we percutaneously applied 0.1% or 1% TC-MTX on the paws and legs of CIA mice and examined parameters reflecting the functions of liver, kidney and bone marrow. There were no differences in blood cell counts and hemoglobin (Hb) levels or in liver and kidney functions among controls, 0.1% and 1% TC-MTX-treated CIA mice (Fig. 6A).

To investigate the toxicity and the signs of skin irritation, various doses of TC-MTX was subcutaneously injected, or percutaneously applied was percutaneously applied or subcutaneously injected on the shaved skin of experimental animals, respectively. No toxicity including animal death or no significant irritation signs were observed (Supplementary material, S2). In addition, Immunotoxicity was not detected in terms of skin sensitization, active systemic anaphylactic shock or passive cutaneous anaphylaxis in Guinea pigs (Supplementary material, S2). The genotoxicity of TC-MTX was not

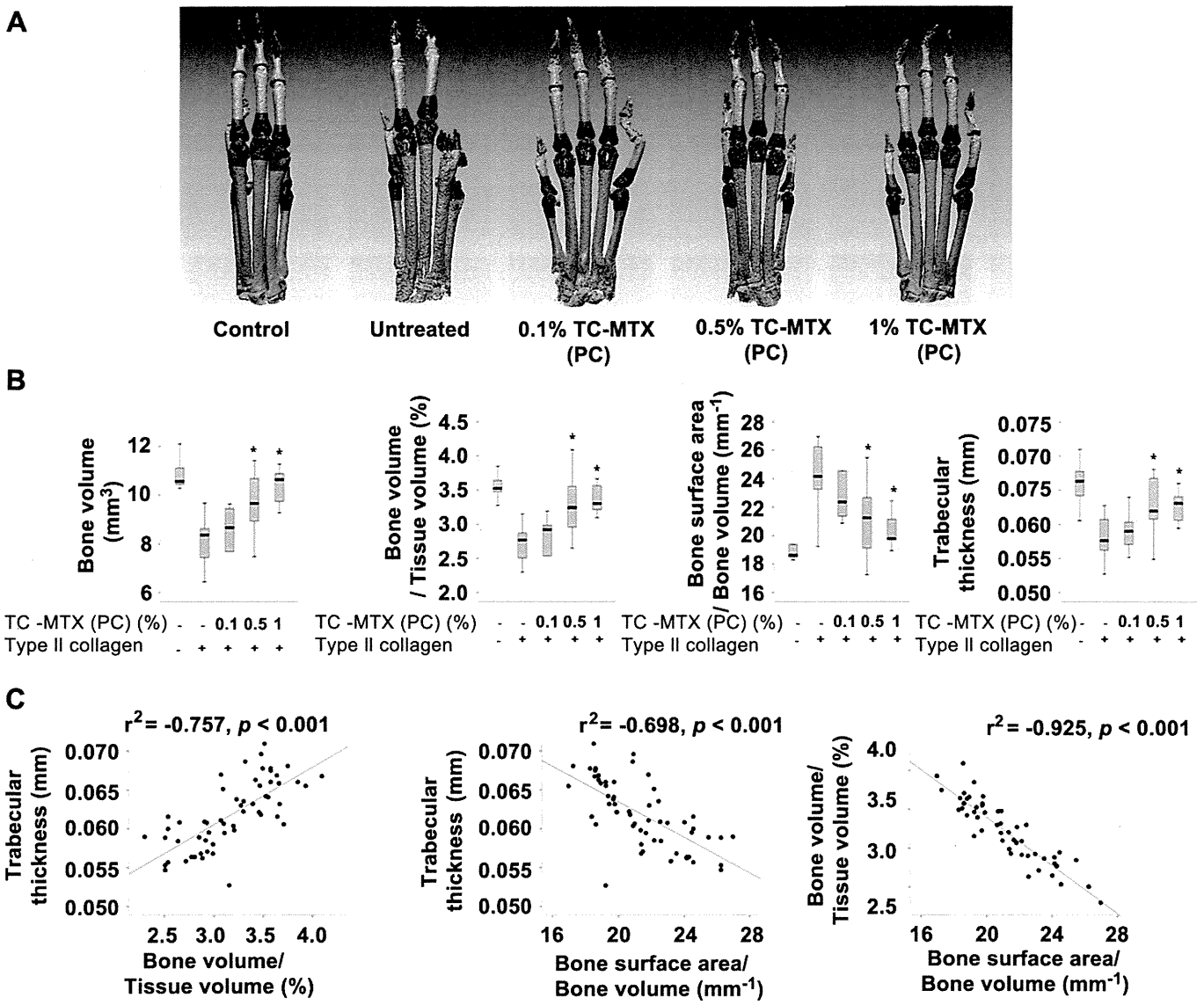

Fig. 3. Micro-CT scan proved efficiency of TC-MTX in CIA mice. Reduced bone destruction and juxta-articular bone loss by 0.1%, 0.5% or 1% transcutaneous MTX (TC-MTX) analyzed by micro-CT scan. Controls were normal mice which did not received type II collagen. Three-dimensional reconstruction of micro-CT imaging of the paws of CIA mice. (PC, percutaneous) (A). Parameters of bone integrity and bone loss (B). Correlation of the parameters obtained from the micro-CT scan (C). Values are given as mean ± SD, $n = 5$, asterisks represent significance compared to untreated mice with $^*p < 0.05$.

observed in the bacterial reverse mutation assay (Supplementary material, S3), the chromosomal aberration test in cultured Chinese Hamster lung cells (Supplementary material, S4) or in the bone marrow micronucleus test in ICR male mice (Supplementary material, S5). Reproductive toxicity was not observed in studies of fertility, embryo-fetal development and pre- and postnatal development (data not shown). Histological changes were examined semi-quantitatively on the skin of CIA mice following the percutaneous administration of TC-MTX. No significant differences were observed in the histological scores among CIA mice percutaneously treated with 0.1% or 1% TC-MTX and controls (Fig. 6b). With these combined results, we conclude that TC-MTX does not induce serious systemic cytotoxic complications.

4. Discussion

MTX is a mainstay for the treatment of RA, but the oral administration of MTX involves risk of systemic and cytotoxic complications. There have been several efforts to develop skin-permeable MTX in order to diminish systemic complications [26,27]. However, no report has been published on the transcutaneous delivery of MTX into joints, or its therapeutic efficacy in an animal model of RA. In this study, we generated a skin-penetrating form of MTX (TC-MTX). The chemical conjugation of Hph-1-PTD and the spacer ACA to a carboxyl group of MTX significantly enhances the solubility of MTX, and the ACA spacer allows MTX to interact comfortably with the binding sites of the substrate without any steric hindrance. There are two carboxyl groups (α and γ positions) available for chemical conjugation in MTX; the α carboxyl group is important for the interaction of MTX to the binding site of DHFR. The poly-glutamation of MTX, which makes MTX toxic to the cells, frequently occurs at the γ position. In agreement with this notion, the inhibitory activity of γ form of TC-MTX on DHFR is comparable to free MTX and higher than the α form of TC-MTX.

The efficiency of the percutaneous delivery of TC-MTX was confirmed in experiments using Franz cells with the hairless mouse skin and human cadaver skin. A low level of MTX delivery was

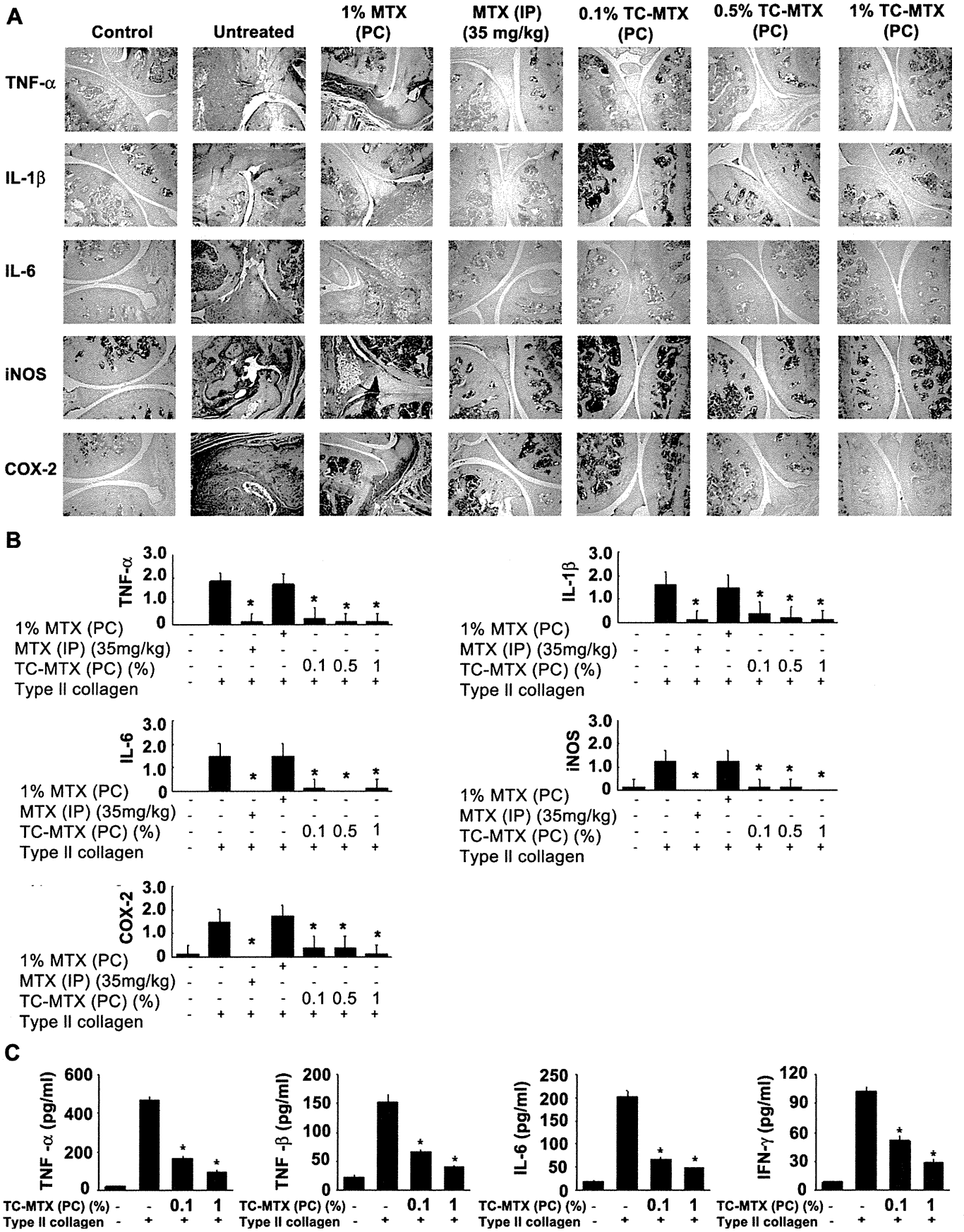

Fig. 4. The level of inflammation-related factors was markedly reduced in inflamed joints and in the serum of CIA mice treated with TC-MTX. Reduced expression of inflammatory cytokines and joint-destructive enzymes in the affected joints and their serum concentrations in CIA mice treated with transcutaneous MTX (TC-MTX). TC-MTX (0.1%, 0.5% or 1%) was percutaneously applied twice per week for five weeks. Controls were normal mice which did not received type II collagen. Immunohistochemical staining for TNF-α, IL-1β, IL-6, iNOS or COX-2 in the joint-sections of CIA mice (original magnification×100). (PC, percutaneous; TC, transcutaneous; IP, intraperitoneal) (A). The semi-quantitative analysis of the degree of stain-positivity of immunohistochemia staining (B). TC-MTX (0.1% or 1%) was percutaneously applied on CIA mice and serum concentrations of TNF-α, IL-1β, IL-6 or IFN-γ were measured (C). Values are given as mean ± SD, $n = 5$, asterisks represent significance compared to untreated mice with $^{*}p < 0.05$.

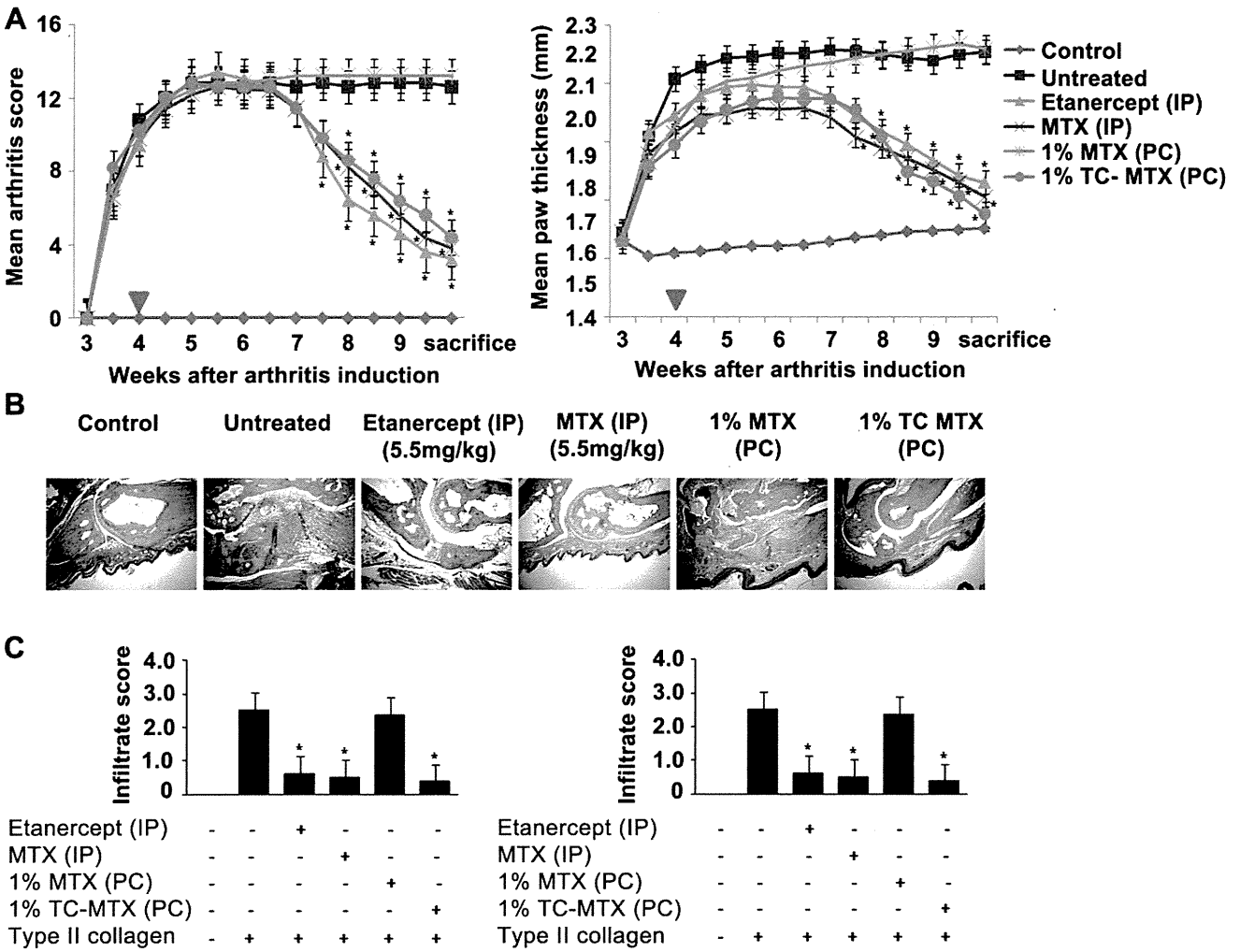

Fig. 5. Comparison of therapeutic efficacy between transcutaneous MTX (TC-MTX) and etanercept. 1% MTX or 1% TC-MTX were applied on the paws and legs of CIA mice, and etanercept (5.5 mg/kg) or MTX (35 mg/kg) were intraperitoneally injected into CIA mice on day 28 after primary immunization (red ▼), twice per week for five weeks. Controls were normal mice which did not received type II collagen. Macroscopic evidence of arthritis such as erythema or swelling was assessed by arthritis score and paw thickness. (PC, percutaneous; IP, intraperitoneal) (A). Histological findings of the joint-sections were evaluated (original magnification×100) (B). The semi-quantitative analysis of histological findings of the inflamed joints such as infiltrate score and erosion score (C). Values are given as mean ± SD, $n = 5$, asterisks represent significance compared to untreated mice with $^{*}p < 0.05$. (For interpretation of the references to colour in this figure legend, the reader is referred to the web version of this article.)

detected in the Franz cell experiment, but this was most likely due to the high pH Tris buffer used to dissolve MTX that damaged the skin layer. When fluorescence-labeled TC-MTX was applied on the joints of mice, it efficiently penetrated the skin in a time-dependent manner, reaching the joints within 24 h after administration. These results clearly demonstrate that TC-MTX can be percutaneously delivered *ex vivo* and *in vivo*, significantly improving the physiochemical properties of MTX.

Table 1
Radioactivity concentration in tissues after a single application of ^{14}C-transcutaneous MTX (TC-MTX) on the skin of non-fasting male rats (dose: 5 mg/kg).

	Radioactivity concentration (ng eq. of TC-MTX/g tissue)				
Tissue	1 h	4 h	24 h	48 h	120 h
Application site	13,213	33,150	31,952	63,745	19,870
Kidney	BLD	BLD	199	186	BLD
Liver	BLD	BLD	73	115	BLD

Upper limit of quantification was 79,045 ng eq. of TC-MTX/g tissue and lower limit of quantification was 40 ng eq. of TC-MTX/g tissue. BLD, below the limit of detection.

TC-MTX ameliorated the severity of arthritis in CIA mice, including marked improvement in the histopathological condition of the joints. Further, there was a significant reduction in inflammatory cell infiltration, synovial hyperplasia, and bone destruction; the decreased levels of TNF-α, IL-1β, IL-6, iNOS, and COX-2 in inflamed joint were also observed. The therapeutic efficacies of TC-MTX were similar to those observed in intraperitoneal MTX-treated CIA mice, in which a substantially higher than the suggested *in vivo* dose of MTX was injected. Moreover, the dose-dependent reduction in the severity of arthritis by TC-MTX provides additional evidence that the improvement was mediated by the pharmacologic action of MTX.

To confirm our results, we measured BV, BV/TV, BS/BV, and Tb.Th, four parameters reflecting the degree of bone destruction and periarticular osteopenia, using highly quantitative micro-CT and three-dimensional reconstruction [28–30]. The typical radiological findings in RA are bone erosions and periarticular osteopenia [31]. The level of bone destruction and periarticular osteopenia due to joint inflammation in CIA mice was quantitatively well correlated with these parameters, supporting the validity of three-dimensional micro-CT. Consistent with our *in vivo* data shown in

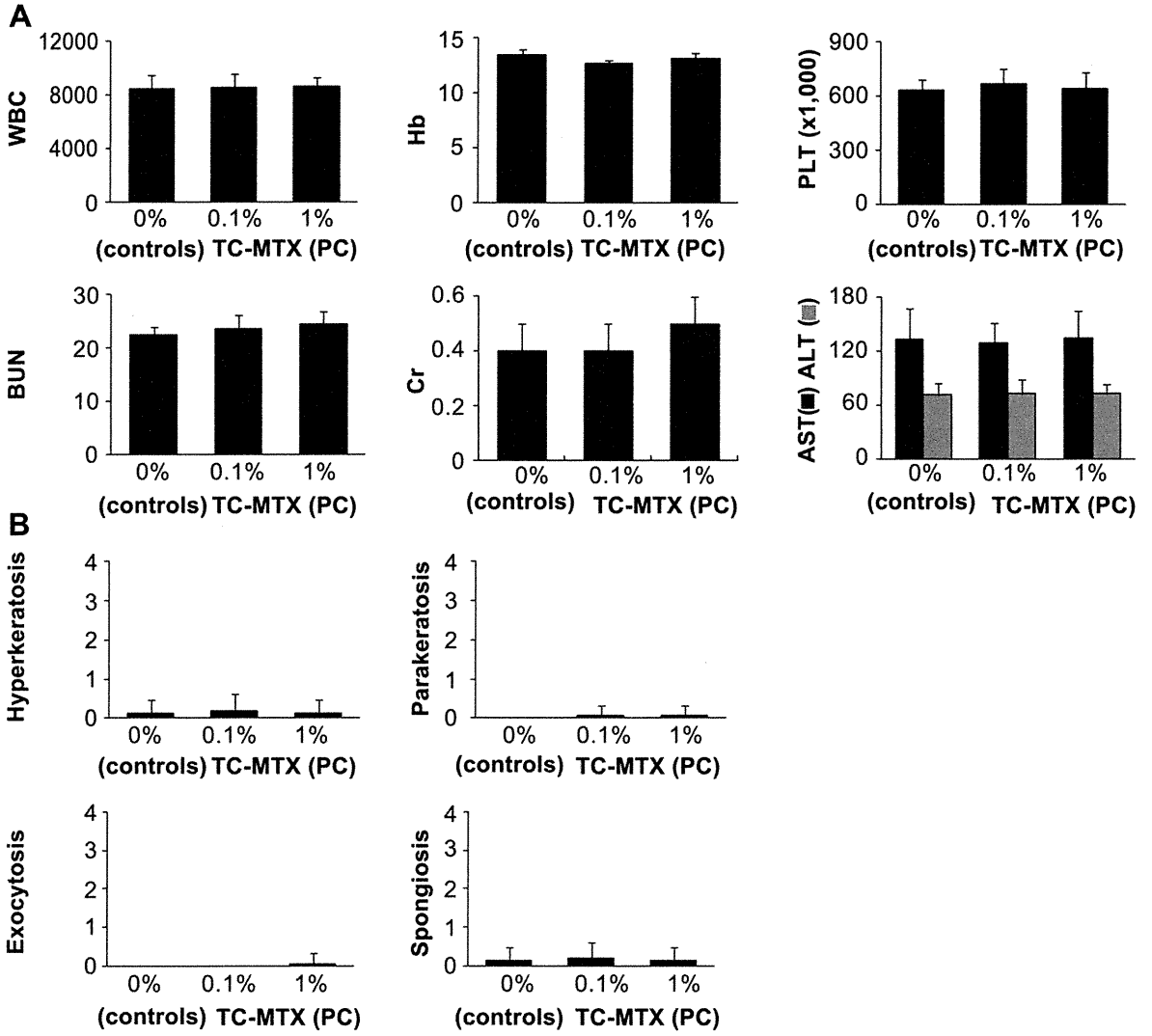

Fig. 6. The cytotoxic effects of transcutaneous MTX (TC-MTX). White blood cell (WBC) count, hemoglobin (Hb), platelet (PLT) count, and the levels of aspartate aminotransferase (AST), alanine aminotransferase (ALT), blood urea nitrogen (BUN), and creatinine (Cr) were examined in blood samples (A). Semi-quantitative analysis of the histological changes on the skin of CIA mice percutaneously treated with TC-MTX (B). Values are given as mean ± SD, $n = 5$, asterisks represent significance compared to untreated mice with $^{*}p < 0.05$.

Figs. 2 and 4, TC-MTX improved all measured parameters in a dose-dependent manner, and the extent of bone preservation by 1% TC-MTX was comparable to that observed in controls.

Biological agents, such as TNF-α blockades or anti-CD20 monoclonal antibody, have been demonstrated to have therapeutic efficacy in RA and are widely used [13,14]. However, they also can induce serious systemic complications. The use of these biological agents must be limited in areas endemic for tuberculosis and viral hepatitis, or in patients suffering from these diseases. In this study, we compared the therapeutic efficacy of TC-MTX to that of etanercept, one of the most widely used biological agents for RA treatment. We found that TC-MTX was comparable to etanercept in the alleviation of arthritis in CIA mice. With these results, we concluded that TC-MTX has similar therapeutic potential to etanercept and it can be safely used in RA patients who have systemic diseases or conditions where the use of biological agents is limited.

In this study, most TC-MTX remained at the application site with significantly low levels of TC-MTX being detected in kidney and liver. In line with these results, systemic complications including genotoxicity, immunotoxicity and skin irritation were not observed. The high toxicity of MTX is caused by the formation of poly-glutamate complexes through the carboxyl group of MTX and the prolonged retention of poly-glutamated MTX in the cytoplasm [32,33]. Hph-1-PTD and ACA occupy the γ-carboxyl group of MTX, where poly-glutamation occurs, leading to the decreased formation of poly-glutamated MTX. The significant reduction of toxicity and the rapid excretion of TC-MTX that was observed was most likely due to enhanced solubility and decreased poly-glutamation of TC-MTX as compared to MTX.

The results of our studies have three important clinical implications in the treatment of RA patients. First, TC-MTX can provide an equivalent level of therapeutic potential to that of oral MTX and etanercept, as well as an opportunity to minimize the circulating concentration of MTX in RA patients who have diseases or conditions that MTX treatment unfeasible such as liver diseases or interstitial lung diseases [11,12]. Second, we observed that most TC-MTX remained at the application site without significant skin irritation, histological changes, or dysfunction in major organs. Thus, it may relieve the concern of rheumatologists that the long-term systemic use of MTX might result in serious complications in RA patients who have refractory small joint inflammation. Third, because TC-MTX allows a high dose of MTX to directly and rapidly

enter the joint cavity, it can reduce the lag-time to the onset of its therapeutic action. Therefore, TC-MTX will reduce irreversible joint destruction and allow better functional status without the concerns of the systemic complications of MTX.

5. Conclusion

Our study demonstrates that TC-MTX can be percutaneously delivered to inflamed joints of CIA mice with similar therapeutic efficiency to that of intraperitoneally injected MTX and -etanercept without the complications associated with the systemic administration of MTX. Thus, TC-MTX may be a new therapeutic modality for RA patients with refractory small joint inflammation or systemic diseases where the use of MTX is unavailable. Furthermore, we expect that TC-MTX can be effectively used to treat other autoimmune inflammatory diseases such as psoriasis, where MTX is one of the first-line drugs.

Acknowledgments

This work was supported in part by Creative Research Initiatives, a National Research Foundation of Korea Grant funded by the Korean Government (2010-0000733) and the Brain Korea 21 (BK21) Program to Sang-Kyou Lee, and the Health & Medical Technology R&D Program by Ministry of Health and Welfare of the Korean Government (2004-A040158) to Soo-Kon Lee. The authors declare no competing financial interests.

Appendix. Supplementary material

Supplementary material associated with this article can be found, in the online version, at doi:10.1016/j.biomaterials.2011.10.079.

References

[1] Choy EH, Panayi GS. Cytokine pathways and joint inflammation in rheumatoid arthritis. N Engl J Med 2001;344:907–16.
[2] Feldmann M, Brennan FM, Maini RN. Role of cytokines in rheumatoid arthritis. Annu Rev Immunol 1996;14:397–440.
[3] Zwerina J, Redlich K, Schett G, Smolen JS. Pathogenesis of rheumatoid arthritis: targeting cytokines. Ann N Y Acad Sci 2005;1051:716–29.
[4] Paulus HE. The use of combinations of disease-modifying antirheumatic agents in rheumatoid arthritis. Arthritis Rheum 1990;33:113–20.
[5] Weinblatt ME, Kaplan H, Germain BF, Merriman RC, Solomon SD, Wall B, et al. Methotrexate in rheumatoid arthritis: effects on disease activity in a multicenter prospective study. J Rheumatol 1991;18:334–8.
[6] Weinblatt ME, Weissman BN, Holdsworth DE, Fraser PA, Maier AL, Falchuk KR, et al. Long-term prospective study of methotrexate in the treatment of rheumatoid arthritis. 84-month update. Arthritis Rheum 1992;35:129–37.
[7] van Riel PL, van der Heijde DM, Nuver-Zwart IH, van de Putte LB. Radiographic progression in rheumatoid arthritis: results of 3 comparative trials. J Rheumatol 1995;22:1797–9.
[8] Mello SB, Barros DM, Silva AS, Laurindo IM, Novaes GS. Methotrexate as a preferential cyclooxygenase 2 inhibitor in whole blood of patients with rheumatoid arthritis. Rheumatology 2000;39:533–6.
[9] Perkins DJ, St Clair EW, Misukonis MA, Weinberg JB. Reduction of NOS2 overexpression in rheumatoid arthritis patients treated with anti-tumor necrosis factor alpha monoclonal antibody (cA2). Arthritis Rheum 1998;41:2205–10.
[10] Schnabel A, Gross WL. Low-dose methotrexate in rheumatic diseases—efficacy, side effects, and risk factors for side effects. Semin Arthritis Rheum 1994;23:310–27.
[11] Kremer JM, Alarcón GS, Lightfoot Jr RW, Willkens RF, Furst DE, Williams HJ, et al. Methotrexate for rheumatoid arthritis. Suggested guidelines for monitoring liver toxicity. American College of Rheumatology. Arthritis Rheum 1994;37:316–28.
[12] van Ede AE, Laan RF, Blom HJ, De Abreu RA, van de Putte LB. Methotrexate in rheumatoid arthritis: an update with focus on mechanisms involved in toxicity. Semin Arthritis Rheum 1998;27:277–92.
[13] Scott DL, Kingsley GH. Tumor necrosis factor inhibitors for rheumatoid arthritis. N Engl J Med 2006;355:704–12.
[14] Silverman GJ, Weisman S. Rituximab therapy and autoimmune disorders: prospects for anti-B cell therapy. Arthritis Rheum 2003;48:1484–92.
[15] Curtis JR, Xi J, Patkar N, Xie A, Saag KG, Martin C. Drug-specific and time-dependent risks of bacterial infection among patients with rheumatoid arthritis who were exposed to tumor necrosis factor alpha antagonists. Arthritis Rheum 2007;56:4226–7.
[16] Kavanaugh AF. B cell targeted therapies: safety considerations. J Rheumatol 2006;(Suppl 77):18–23.
[17] Sfikakis PP. The first decade of biologic TNF antagonists in clinical practice: lessons learned, unresolved issues and future directions. Curr Dir Autoimmun 2010;11:180–210.
[18] Bartelds GM, Wijbrandts CA, Nurmohamed MT, Stapel S, Lems WF, Aarden L, et al. Clinical response to adalimumab: relationship to anti-adalimumab antibodies and serum adalimumab concentrations in rheumatoid arthritis. Ann Rheum Dis 2007;66:921–6.
[19] Radstake TR, Svenson M, Eijsbouts AM, van den Hoogen FH, Enevold C, van Riel PL, et al. Formation of antibodies against infliximab and adalimumab strongly correlates with functional drug levels and clinical responses in rheumatoid arthritis. Ann Rheum Dis 2009;68:1739–45.
[20] Schreiber S, Mahmoud A, Vuia A, Rübbelke MK, Schmidt E, Schaller M, et al. Reconstructed epidermis versus human and animal skin in skin absorption studies. Toxicol in Vitro 2005;19:813–22.
[21] Lee SW, Kim JH, Park YB, Lee SK. Bortezomib attenuates murine collagen-induced arthritis. Ann Rheum Dis 2009;68:1761–7.
[22] Shen T, Zhu QX, Yang S, Wu CH, Zhang HF, Zhou CF, et al. Trichloroethylene induced cutaneous irritation in BALB/c hairless mice: histopathological changes and oxidative damage. Toxicology 2008;248:113.
[23] Parfitt AM, Drezner MK, Glorieux FH, Kanis JA, Malluche H, Meunier PJ, et al. Bone histomorphometry: standardization of nomenclature, symbols, and units. Report of the ASBMR Histomorphometry Nomenclature Committee. J Bone Miner Res 1987;2:595–610.
[24] Delgado M, Abad C, Martinez C, Leceta J, Gomariz RP. Vasoactive intestinal peptide prevents experimental arthritis by downregulating both autoimmune and inflammatory components of the disease. Nat Med 2001;7:563–8.
[25] Gonzalez-Rey E, Fernandez-Martin A, Chorny A, Delgado M. Vasoactive intestinal peptide induces CD4+, CD25+ T regulatory cells with therapeutic effect in collagen- induced arthritis. Arthritis Rheum 2006;54:864–76.
[26] Chatterjee DJ, Li WY, Koda RT. Effect of vehicles and penetration enhancers on the in vitro and in vivo percutaneous absorption of methotrexate and edatrexate through hairless mouse skin. Pharm Res 1997;14:1058–65.
[27] Wong TW, Zhao YL, Sen A, Hui SW. Pilot study of topical delivery of methotrexate by electroporation. Br J Dermatol 2005;152:524–30.
[28] Back KH, Lee WP, Diehl LJ, Ross J, Gribling P, Zhang Y, et al. Quantification of cortical bone loss and repair for therapeutic evaluation in collagen-induced arthritis, by micro-computed tomography and automated image analysis. Arthritis Rheum 2004;50:3377–86.
[29] Botter SM, van Osch GJ, Waarsing JH, Day JS, Verhaar JA, Pols HA, et al. Quantification of subchondral bone changes in a murine osteoarthritis model using micro-CT. Biorheology 2006;43:379–88.
[30] Swieszkowski W, Tuan BH, Kurzydlowski KJ, Hutmacher DW. Repair and regeneration of osteochondral defects in the articular joints. Biomol Eng 2007;24:489–95.
[31] Goldring SR, Gravallese EM. Pathogenesis of bone erosions in rheumatoid arthritis. Curr Opin Rheumatol 2000;12:195–9.
[32] Chabner BA, Allegra CJ, Curt GA, Clendeninn NJ, Baram J, Koizumi S, et al. Polyglutamation of methotrexate. Is methotrexate a prodrug? J Clin Invest 1985;76:907–12.
[33] Fry DW, Anderson LA, Borst M, Goldman ID. Analysis of the role of membrane transport and polyglutamation of methotrexate in gut and the Ehrlich tumor in vivo as factors in drug sensitivity and selectivity. Cancer Res 1983;43:1087–92.

RESEARCH ARTICLE

Human Mutation

OFFICIAL JOURNAL
HGVS
HUMAN GENOME VARIATION SOCIETY
www.hgvs.org

Functional Characterization and Targeted Correction of ATM Mutations Identified in Japanese Patients with Ataxia-Telangiectasia

Kotoka Nakamura,[1] Liutao Du,[1] Rashmi Tunuguntla,[1] Francesca Fike,[1] Simona Cavalieri,[2] Tomohiro Morio,[3] Shuki Mizutani,[3] Alfredo Brusco,[2] and Richard A. Gatti[1,4]*

[1]*Department of Pathology and Laboratory Medicine, UCLA School of Medicine, Los Angeles, California;* [2]*Department of Genetics, Biology and Biochemistry, University of Torino, Medical Genetics Unit, S. Giovanni Battista Hospital, Torino, Italy;* [3]*Department of Pediatrics and Developmental Biology, Tokyo Medical and Dental University Graduate School of Medicine, Tokyo, Japan;* [4]*Department of Human Genetics, UCLA School of Medicine, Los Angeles, California*

Communicated by Michel Goossens

Received 14 June 2011; accepted revised manuscript 15 September 2011.
Published online 17 October 2011 in Wiley Online Library (www.wiley.com/humanmutation).DOI: 10.1002/humu.21632

ABSTRACT: A recent challenge for investigators studying the progressive neurological disease ataxia-telangiectasia (A-T) is to identify mutations whose effects might be alleviated by mutation-targeted therapies. We studied ATM mutations in eight families of Japanese A-T patients (JPAT) and were able to identify all 16 mutations. The probands were compound heterozygotes in seven families, and one (JPAT2) was homozygous for a frameshift mutation. All mutations—four frameshift, two nonsense, four large genomic deletions, and six affecting splicing—were novel except for c.748C>T found in family JPAT6 and c.2639-384A>G found in family JPAT11/12. Using an established lymphoblastoid cell line (LCL) of patient JPAT11, ATM protein was restored to levels approaching wild type by exposure to an antisense morpholino oligonucleotide designed to correct a pseudoexon splicing mutation. In addition, in an LCL from patient JPAT8/9, a heterozygous carrier of a nonsense mutation, ATM levels could also be partially restored by exposure to readthrough compounds (RTCs): an aminoglycoside, G418, and a novel small molecule identified in our laboratory, RTC13. Taken together, our results suggest that screening and functional characterization of the various sorts of mutations affecting the *ATM* gene can lead to better identification of A-T patients who are most likely to benefit from rapidly developing mutation-targeted therapeutic technologies.

Hum Mutat 33:198–208, 2012. © 2011 Wiley Periodicals, Inc.

KEY WORDS: ataxia-telangiectasia; ATM; large genomic deletions; functional analysis of DNA variants; mutation-targeted therapy; Japanese ATM mutation

Introduction

Ataxia-telangiectasia (A-T; MIM# 208900) is an autosomal recessive neurodegenerative disorder characterized by progressive cerebellar degeneration, ocular apraxia and telangiectasia, increased cancer risk, immunodeficiency, sensitivity to ionizing radiation (IR), chromosomal instability, and cell cycle abnormalities [Boder and Sedgwick, 1958; Gatti, 2001]. A-T is caused by mutations in the *ATM* gene (MIM# 607585) that usually encodes a 13 kb transcript that produces a 370 kDa protein [Gatti et al., 1988; Lange et al., 1995; Savitsky et al., 1995]. Intranuclear ATM protein is low or absent in most A-T patients, despite the presence of relatively normal levels of *ATM* transcripts. ATM is activated by autophosphorylation after binding with the MRN (Mre11-Rad50-Nbs) complex at sites of DNA double strand breaks [Bakkenist and Kastan, 2003; Kozlov et al., 2006], and subsequently phosphorylates hundreds of downstream target proteins involved in cell cycle checkpoints, DNA repair, and apoptosis [Bolderson et al., 2009; Matsuoka et al., 2007; Shiloh 2006]. ATM also appears to play a critical role in resolving chronic inflammation [Westbrook and Schiestl, 2010].

A-T patients are usually compound heterozygotes, carrying two distinct mutations. Mutations occur throughout the entire gene without hot spots. Founder effects are commonly observed in many ethnic isolates [Birrell et al., 2005; Campbell et al., 2003; Cavalieri et al., 2006; Gilad et al., 1996a; Laake et al., 1998; McConville et al., 1996; Mitui et al., 2003, 2005; Telatar et al., 1998a, b] wherein patients often carry mutations in a homozygous state. We have previously shown [Du et al., 2007, 2009, 2011; Lai et al., 2004] that accurately analyzing the functional consequences of mutations in individual A-T patients enables the grouping of patients into "mutation categories" that are most likely to be corrected by future customized mutation-targeted therapies.

The aims of the present study were to: (1) characterize the *ATM* mutations in Japanese A-T (JPAT) families; and (2) identify which JPAT patients might be candidates for personalized mutation-targeted therapy. We report that three of eight JPAT families examined are potential candidates for mutation-targeted therapy based on partial restoration of functional ATM protein production.

Materials and Methods

Cell Lines

Lymphoblastoid cell lines (LCLs) [Svedmyr et al., 1975] or activated T-cells [Minegishi et al., 2006] were established from affected

Additional Supporting Information may be found in the online version of this article.

*Correspondence to: Richard A. Gatti, Department of Pathology and Laboratory Medicine, UCLA School of Medicine, 675 Charles E. Young Drive South, Los Angeles, CA 90095-1732. E-mail: rgatti@mednet.ucla.edu

Contract grant sponsors: National Institutes of Health (1R01NS052528); A-T Ease Foundation; A-T Medical Research Foundation.